



## Bedrock channel geometry along an orographic rainfall gradient in the upper Marsyandi River valley in central Nepal

William H. Craddock,<sup>1,2</sup> Douglas W. Burbank,<sup>1</sup> Bodo Bookhagen,<sup>3</sup> and Emmanuel J. Gabet<sup>4</sup>

Received 7 June 2006; revised 9 March 2007; accepted 31 March 2007; published 25 July 2007.

[1] Pronounced rainfall gradients combined with spatially uniform exhumation of rocks at Quaternary timescales and uniform rock strength make the upper Marsyandi River valley in central Nepal a useful natural laboratory in which to explore variations in bedrock channel width. We focus on small catchments (0.6–12.4 km<sup>2</sup>) along a more than tenfold gradient in monsoon rainfall. Rainfall data are gathered from a dense weather network and calibrated satellite observations, the pattern of Quaternary exhumation is inferred from apatite fission track cooling ages, and rock compressive strength is measured in the field. Bedrock channel widths, surveyed at high scour indicators, scale as a power law function of discharge ( $w \propto Q_w^{0.38 \pm 0.09}$ ) that is estimated by combining rainfall data with 90-m digital topography. The results suggest that power law width scaling models apply (1) to regions with pronounced rainfall gradients, (2) to tributary catchments distributed across a climatically diverse region, and (3) to large, rapidly denuding orogens. An analysis of rainfall data indicates that the regional gradient of rainfall during storms that drive erosive discharge events is about half as large as the gradient of seasonal rainfall across the same area. Finally, numerical models in which the maximum rainfall is displaced significantly downstream from the headwaters predict a midcatchment zone of relatively rapid decreases in channel gradient and increases in channel concavity that are driven by locally enhanced discharge. Because differential rock uplift can produce analogous changes in gradients, the influence of rainfall gradients should be assessed before tectonic inferences are drawn.

**Citation:** Craddock, W. H., D. W. Burbank, B. Bookhagen, and E. J. Gabet (2007), Bedrock channel geometry along an orographic rainfall gradient in the upper Marsyandi River valley in central Nepal, *J. Geophys. Res.*, *112*, F03007, doi:10.1029/2006JF000589.

### 1. Introduction

[2] Observations of concurrent late Cenozoic climate change and uplift of rocks across the globe inspired a debate about whether rock uplift led to climate change or vice versa [Molnar and England, 1990; Raymo and Ruddiman, 1992]. The debates soon gave way to modeling studies investigating geodynamic and surface-process coupling [Howard *et al.*, 1994; Small and Anderson, 1995; Kooi and Beaumont, 1996; Willett, 1999]. Within the last 5 years, several empirical studies have attempted to test some of the predictions of coupled geodynamic-surface process models [Burbank *et al.*, 2003; Dadson *et al.*, 2003; Reiners *et al.*, 2003; Wobus *et al.*, 2003, 2005]. Mountain river networks

play an integral role in coupling surface processes to geodynamics because they route water, delivered as precipitation, through a landscape, erode bedrock, and redistribute sediment [Howard *et al.*, 1994]. Over geologic timescales (10<sup>6</sup>–10<sup>8</sup> years), the removal of mass from the top of actively deforming orogens alters the distribution of stress across the range [Willett, 1999]. Moreover, rivers set the local base level of erosion for adjacent hillslopes, thereby modulating hillslope angles and stability. In rapidly denuding landscapes, the rate of river lowering dictates the overall rate of hillslope erosion [Burbank, 2002]. Consequently, knowledge of the characteristics, controls, and processes of mountain river systems underpins understanding of landscape evolution [Whipple, 2004].

[3] In this study, we combine meteorological records from the Marsyandi valley in Nepal, detailed measurements of bedrock channel width, and numerical models in order to address three problems concerning the geometry of mountain river channels and the evolution of rapidly denuding orogenic landscapes characterized by pronounced rainfall gradients. First, we examine spatial changes in bedrock channel width across a more than tenfold rainfall gradient. Most recent studies that assessed the width of bedrock channels as a function of discharge [Montgomery and Gran,

<sup>1</sup>Department of Earth Science, University of California, Santa Barbara, Santa Barbara, California, USA.

<sup>2</sup>Now at Department of Geosciences, Pennsylvania State University, University Park, Pennsylvania, USA.

<sup>3</sup>Department of Geological and Environmental Sciences, Stanford University, Stanford, California, USA.

<sup>4</sup>Department of Environmental Science, University of California, Riverside, Riverside, California, USA.

2001; Snyder *et al.*, 2003a; Duvall *et al.*, 2004; Wohl *et al.*, 2004] did so in regions with subdued or poorly known spatial gradients in rainfall. With a focus on small tributary catchments, we find systematic, discharge-related changes in width, such that narrower channels in drier areas effectively focus the erosive power of rivers onto a smaller area of the channel bed, tending to increase the rate of vertical fluvial incision.

[4] Second, in the context of a simple stream power model, we compare spatial patterns of erosion driven by (1) individual storms and (2) rainfall averaged over several years. The pronounced gradient in annual monsoon rainfall across the Marsyandi valley has led past researchers to predict corresponding large gradients in erosion rates [Burbank *et al.*, 2003]. Given that moderate to large floods generally do the bulk of the geomorphic work [e.g., Leopold and Maddock, 1953], spatial gradients in the magnitude and frequency of such large events are more likely than average seasonal rainfall to control landscape evolution [e.g., Gabet and Dunne, 2003]. Thus the erosion of a landscape should be set by the distribution of large storms and not average rainfall. Nonetheless, in many studies of mountainous regions for which climatic data are available, annual or seasonal averages are used to characterize spatial variations in rainfall [e.g., Reiners *et al.*, 2003] and hence both discharge and stream power. In this study, we use rainfall records, typically 5 or 6 years long, with half hourly data at 18 sites from the Marsyandi valley to investigate the distribution of rainfall during storms in the central Himalaya. We show that, during 5-day storms that recur 1–5 times per year, spatial gradients in rainfall are about half as large as those found for average monsoon rainfall. This difference suggests that apparent contrasts across the Himalaya in predicted erosion as a function of stream power are not as great as previously described [e.g., Burbank *et al.*, 2003].

[5] Third, we examine the theoretical impact on longitudinal river profiles of a rainfall maximum that is displaced significantly downstream of the catchment headwaters. Previous work has explored river longitudinal profiles in the context of rainfall that either increases or decreases toward the headwaters of catchment [Roe *et al.*, 2002, 2003]. In large orogens, rainfall maxima tend to correlate with thresholds in topographic relief and can be displaced many kilometers upwind of drainage divides [Roe *et al.*, 2003; Anders *et al.*, 2006; Bookhagen and Burbank, 2006]. Using idealized catchments and rainfall distributions from the Himalaya, we predict a rapid decrease in the slope of the trunk stream in and around the zone of maximum precipitation. Whereas such a trend might be interpreted to result from differential rock uplift or variations in rock strength [Snyder *et al.*, 2000; Kirby *et al.*, 2003; Duvall *et al.*, 2004], our results show that these changes can also derive solely from rainfall gradients.

## 2. Marsyandi Valley Field Area

[6] The Marsyandi River is a transverse river that flows perpendicular to the strike of the Himalaya (Figure 1). The headwaters are located on the southern margin of the Tibetan Plateau, which is composed of Paleozoic and Mesozoic sedimentary rocks and low-grade metasedimen-

tary rocks [Hodges *et al.*, 1996; Searle and Godin, 2003] (Figure 1a). Downstream, the river crosses two strands of the South Tibetan Detachment Fault (STD): one which is represented by the Chame Detachment and the other by the Phu Detachment (PD) in the eastern part of the study area (Figure 1a). The latter circumscribes a large portion of the Nar drainage basin [Searle and Godin, 2003] (Figure 1b). After crossing the STD, the Marsyandi cuts the Proterozoic and lower Paleozoic Greater Himalayan Sequence (GHS) and is flanked to either side by 8000-m peaks. The GHS is subdivided into three units: the lowest unit, Formation I, is a micaceous gneiss; the middle unit, Formation II, is a calcareous gneiss; and the highest unit, Formation III; is an augen gneiss [Searle and Godin, 2003]. Finally, after crossing the Main Central Thrust (MCT), the Marsyandi flows through the Lesser Himalayan Sequence (LHS) and then joins the Trisuli River. The MCT was originally mapped on the basis of lithologic and metamorphic facies criteria [Colchen *et al.*, 1986]. In the Marsyandi region, the Main Central Thrust was active from the Oligocene to the Miocene [Searle and Godin, 2003]. Subsequently, major thrusting was transferred into the Lesser Himalaya in the middle to late Miocene. Geomorphic, structural, and thermochronologic evidence, however, suggest Quaternary deformation on the Main Central Thrust [Huntington *et al.*, 2006; Blythe *et al.*, 2007] and in its proximal footwall [Wobus *et al.*, 2003, 2005; Hodges *et al.*, 2004]. Evidence for post-Miocene deformation has prompted some to define a second, more southerly Main Central Thrust II (Figure 1b) [Searle and Godin, 2003]. Diverse and highly fractured metasedimentary rocks crop out in the LHS, dominantly schist and quartzite. Apatite fission track (AFT) cooling ages [Burbank *et al.*, 2003; Blythe *et al.*, 2007] have been interpreted to reflect rapid and generally spatially uniform rates of exhumation during the last 1 Ma from the MCT to the Phu Detachment (Figure 2b). Increasingly old AFT ages are found to the south of the MCT (Figure 2b).

[7] A weather network consisting of 18 stations measuring rainfall half hourly was in place from 1999 to 2003 with more limited data from 2004 in and near the Marsyandi drainage basin [Barros *et al.*, 2000]. Roughly three quarters of the total annual rainfall at any given station falls during the monsoon. Limited data suggest that rainfall totals in the southern margin of the study area are  $\sim 1.0$  m during the summer monsoon months (June–September) (Figure 2c). As moist air is orographically lifted at the High Himalayan topographic front, mean annual monsoon rainfall abruptly increases to  $\sim 3.5$  m at an average elevation of  $\sim 2000$ – $3000$  m. A key feature of the orographic gradient is that the rainfall maximum is offset to the south of the crest of the Himalaya by  $\sim 15$  km (Figure 2c). North of the rainfall maximum, rainfall steadily decreases to  $\sim 0.3$  m per monsoon. Thus monsoon rainfall totals decrease by over an order of magnitude over  $\sim 30$  km distance. If the fission track ages across the Greater Himalaya [Blythe *et al.*, 2007] can be viewed as a proxy for long-term erosion rates, then the absence of a significant south-to-north gradient in cooling ages stands in sharp contrast to the pronounced rainfall gradient across the same area (Figure 2). This apparent decoupling of patterns of modern rainfall from gradients in long-term erosion [Burbank *et al.*, 2003] poses

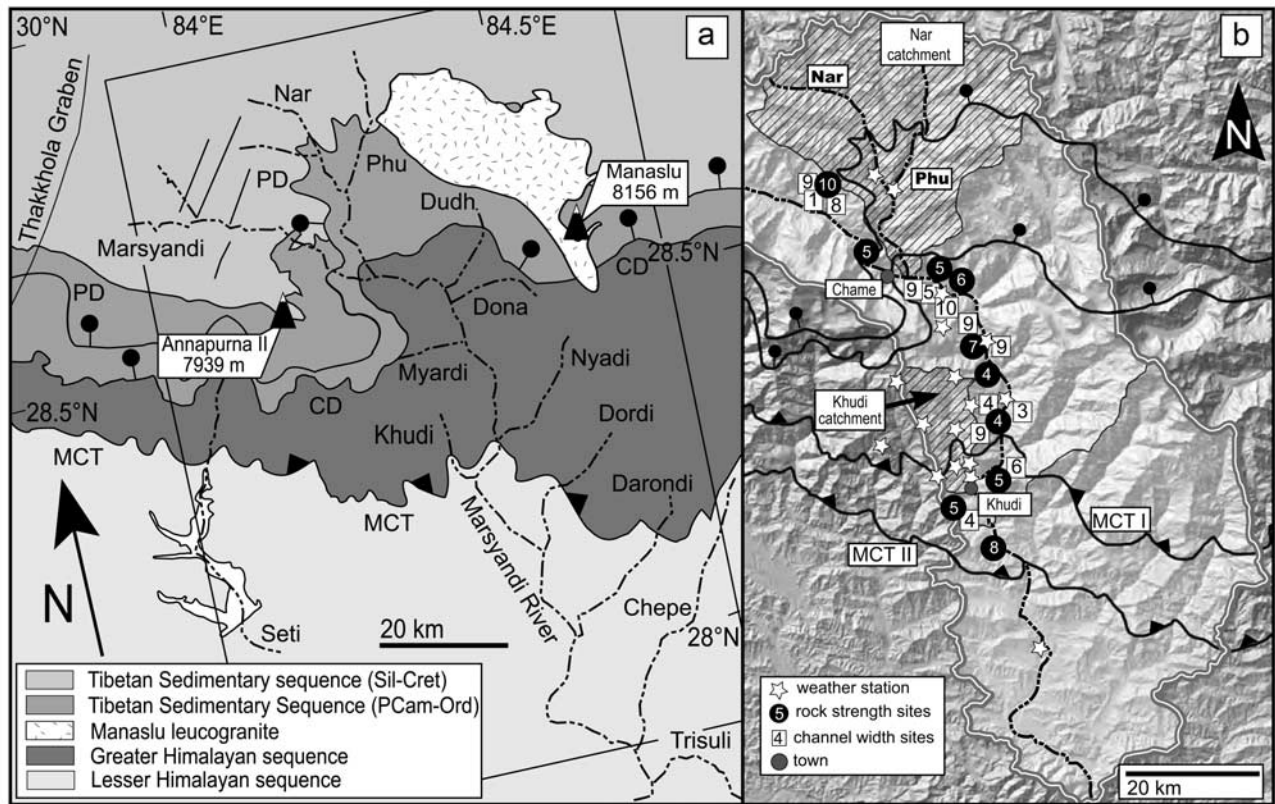


**Figure 1.** (a) Geologic map of Annapurna region after *Brewer et al.* [2006] and *Searle and Godin* [2003]. Study area shown in box. PD, Phu Detachment; CD, Chame Detachment; MCT, Main Central Thrust. (b) Marsyandi catchment with locations of weather stations (stars), channel width measurement sites (boxes), and rock strength measurement sites (circles). Numbers inside black circles/white boxes indicate the number of rock strength measurement sites/channel width measurement sites in the area. Nar, Khudi, and upper Marsyandi catchment and the towns of Khudi and Chame are shown.

a challenge to models and interpretations in which rainfall and erosion rates are correlated [e.g., *Reiners et al.*, 2003].

[8] A network of 10 stream gauges provides water discharge data along the Marsyandi and for a few tributaries. For most of the year, the discharge at each station is low. Discharge increases as the monsoon begins to intensify in May, maximizes during the monsoon months of June–September, and, beginning in October and November, tapers to winter base flow levels. About 1–10 times during the monsoon season, discharges  $\geq 50\%$  larger than mean monsoon flows occur. Such events typically correspond to consecutive rainy days. In relatively small catchments, storms cause more pronounced discharge spikes than in larger catchments.

[9] Numerous small catchments ( $< 30 \text{ km}^2$ ) drain the slopes adjacent to the Marsyandi. Hillslopes throughout the landscape are steepened to critical angles for failure [*Burbank et al.*, 1996] as indicated by abundant field evidence of bedrock landslides [*Gabet et al.*, 2004b] and correlations of hillslope angles with rainfall amounts [*Gabet et al.*, 2004a]. On the basis of 90-m SRTM and DTED digital elevation models (DEMs), an analysis of channel segments  $\geq 500 \text{ m}$  long in 3–20  $\text{km}^2$  catchments demonstrates that the channels are very steep, with reach-average slopes commonly  $\geq 0.35 \text{ m/m}$  [*Burbank et al.*, 2003]. The channels are bedrock or mixed bedrock-alluvial, and at low

flow are most commonly mantled with a sediment veneer ranging from sand to boulders. Whereas erosion at Quaternary timescales appears rather uniform across the breadth of Greater Himalaya [*Burbank et al.*, 2003], tributaries to this stretch of the Marsyandi receive strikingly different amounts of monsoon rainfall, making the upper Marsyandi River valley an intriguing location, well suited for a study of channel geometry along a climate gradient.

### 3. Erosion and Scaling in Bedrock Rivers

[10] In some natural settings, the suite of processes responsible for eroding bedrock channels may be represented by models based on unit stream power [*Howard et al.*, 1994; *Hancock et al.*, 1998; *Whipple and Tucker*, 1999; *Whipple et al.*, 2000]. In its simplest expression, the stream-power model states that rates of bedrock river incision ( $E$ ) are linearly related to stream power per unit area of channel bed using the following expression:

$$E = k\rho gQS/w, \quad (1)$$

where  $k$  is a coefficient related to the erodibility of the substrate,  $\rho$  is the density of the water in the river channel,  $g$  is gravitational acceleration,  $Q$  is the discharge of the channel,  $S$  is the channel slope, and  $w$  is channel width. This

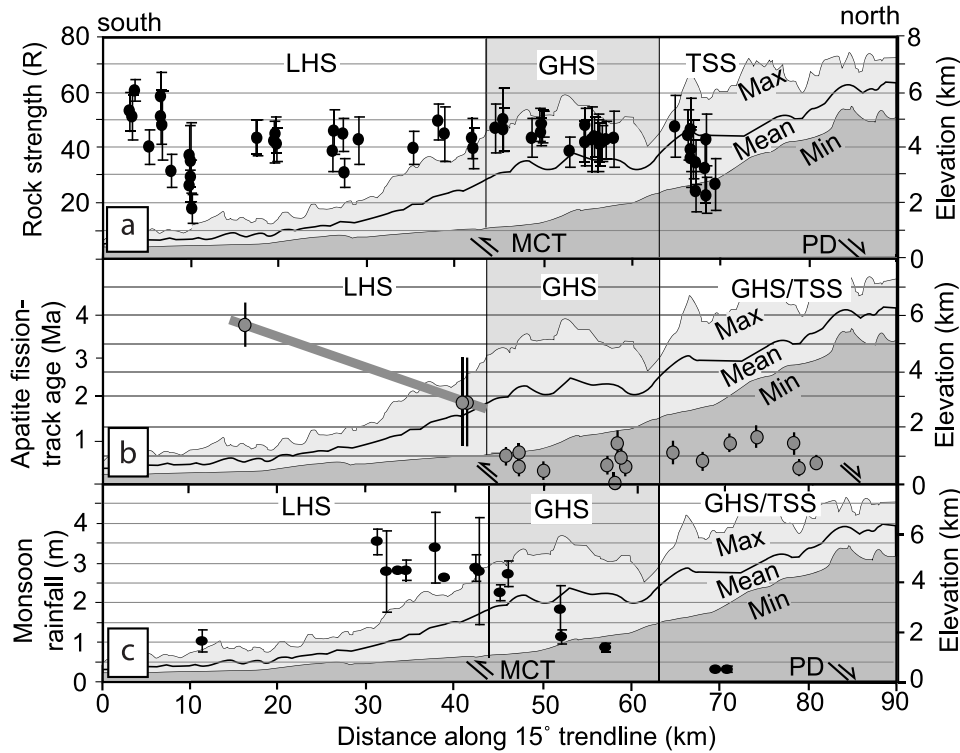


**Figure 2.** Data for cross-Himalaya transect oriented  $15^\circ\text{E}$  through the study area. (a) Mean Schmidt hammer measurements with  $1\sigma$  errors plotted against topography and main lithotectonic zones. (b) Apatite fission track cooling ages [Blythe *et al.*, 2007] plotted above maximum, minimum, and mean topography along a  $15^\circ$  trend. (c) Mean annual monsoon rainfall (dots) plotted above maximum, mean, and minimum topography along a  $15^\circ$  trend. Error bars on rainfall are  $1\sigma$  and greater error bars reflect greater seasonal variations. GHS, Greater Himalayan Sequence; LHS, Lesser Himalayan Sequence; TSS, Tibetan Sedimentary Series; PD, Phu Detachment.

model is often simplified by subsuming the constants,  $k$ ,  $\rho$ , and  $g$  into one constant,  $K$ , and by expressing  $w$  as a function of  $Q$  [Leopold and Maddock, 1953]. By adding exponents,  $m$  and  $n$ , to the discharge and slope terms respectively, the assumption that river incision is related to unit stream power can be relaxed, and the commonly applied model for river incision is obtained,

$$E = KQ^m S^n. \quad (2)$$

[11] In landscape-scale fluvial studies that are relevant to orogenic evolution, several assumptions are typically employed to facilitate estimates of the erosive role of rivers. Width is assumed to scale as a power of discharge,

$$w = k_w Q^b, \quad (3)$$

where  $k_w$  and  $b$  are empirical constants. In alluvial channels and in varying climatic regimes,  $b$  is typically  $\sim 0.5$  [Knighton, 1998, and references therein]. Because discharge in individual rivers is poorly known in many landscape studies, discharge is commonly expressed as a function of upstream drainage area,  $A$ , such that

$$Q = k_q A^c, \quad (4)$$

where  $k_q$  and  $c$  are empirical constants. For drainage basins with limited orographic effects and homogeneous vegeta-

tion, the value of  $c$  is assumed to be  $\sim 1$ , and  $k_q$  is assumed to be uniform on a regional scale, such that discharge and drainage area are linearly related and roughly interchangeable [Knighton, 1998; Snyder *et al.*, 2003a]. Most recent studies that assessed the width of bedrock channels as a function of discharge [Montgomery and Gran, 2001; Snyder *et al.*, 2003a; Duvall *et al.*, 2004; Wohl *et al.*, 2004] did so in regions with subdued or poorly known spatial gradients in rainfall, such that it was reasonable and/or necessary to use  $A$  as a proxy for  $Q$ . In individual, small drainage basins ( $< 15 \text{ km}^2$ ), such as those studied here, orographic rainfall gradients are commonly modest, and  $c$  may be  $\sim 1$ . However,  $k_q$  cannot be the same for two nearby catchments draining an equal area, but receiving strikingly different amounts of rainfall. Moreover, in larger catchments draining 100s to 1000s  $\text{km}^2$  and displaying pronounced rainfall gradients, the value of  $c$  will depart from 1. Given the reasonable expectation that drainage area and discharge are not related linearly in the Himalaya and high-resolution rainfall measurements, we compare width to discharge in this study.

## 4. Methods

### 4.1. Field Methods

[12] The texture of an orogenic landscape requires that a large portion of the total erosion occurs within small drainage basins. Therefore river incision laws should be

**Table 1.** Smallest and Largest Floods Likely to Set High Scour Marks in the Marsyandi Valley<sup>a</sup>

	Temang	Danaque	Khudi
Q <sub>3</sub> week, m <sup>3</sup> /day	480000	130000	6500000
Q <sub>2</sub> year, m <sup>3</sup> /day	670000	190000	17000000
Q <sub>3</sub> week/Q <sub>2</sub> year	0.72	0.68	0.38
Q <sub>3</sub> week <sup>0.26</sup> /Q <sub>2</sub> year <sup>0.26</sup>	0.92	0.90	0.78

<sup>a</sup>The 3-week monsoon season and 2-year flood are used as estimates of the smallest and largest events likely to set high scour marks in a channel. The magnitude and channel width of the two floods are compared for three rivers: the Temang Khola (19 km<sup>2</sup>), the Danaque Khola (6 km<sup>2</sup>), and the Khudi Khola (130 km<sup>2</sup>).

calibrated to small basins. We restricted our channel-width measurements to sites in tributary catchments draining between 0.6 and 12.4 km<sup>2</sup>. Following *Montgomery and Gran* [2001], width measurements were made at the highest level on the channel margin showing evidence of recent scour, commonly indicated by vegetation trimlines, but also by sediment trimlines, staining, and/or tool marks. A clear indication of high scour and the nature of the bank were key criteria for site selection. Although most measurements of channel width were made at bedrock sites, some mixed bedrock-alluvial sites were included if the bank material appeared to be stationary on timescales much greater than the mean annual flood. Thus, where boulders exceeded ~3 m diameter on one bank and the other wall was bedrock, the channel was considered as a bedrock channel. At each of 71 sites, 3–4 channel width measurements were made with a laser range finder and/or a tape measure. Width measurements at a site were generally reproducible to within 10 cm. At each site, 2–3 longitudinal river profiles were surveyed along the water surface, usually over a distance of ~2–10 channel widths, such that each profile contains ~20–50 points and its upstream and downstream limits are defined by breaks in channel slope. The survey points were projected onto a line and a linear regression was used to define channel gradient. For a few sites, a hand inclinometer was used to measure slope.

[13] In order to constrain spatial variations in rock strength, rock compressive strength was quantified with a Schmidt hammer on relatively unweathered bedrock surfaces at channel-width sites and other outcrops, generally steep cliff faces. Individual measurements returning values <10 *R* probably indicate highly weathered or fractured rock and were discarded. Consequently, intact, but weak rock was not measured with this method. At each site, 40 measurements were made at 10- to 20-cm intervals, along 4 transects containing 10 measurements each.

#### 4.2. Uncertainty in Channel Width Measurements

[14] The validity of channel-width measurements is affected by measurement error, along-channel width variability, and uncertainties about the reference discharge. Given that laser-ranger measurements are reproducible to ~10 cm and channel width measurements were 1–10 m, we estimate the measurement error to be <10% for a single cross-channel profile. Given the diverse width-depth ratios of mountain rivers [*Montgomery and Buffington*, 1997], we tried to reduce uncertainties by avoiding pools, choosing

reaches of relatively uniform width, and making replicate measurements. The mean standard deviation for 3–4 width profiles at a site is 12%. Uncertainty also results from the difficulty of defining a reference discharge, such as the mean annual flood, at which to measure bedrock channel width [*Montgomery and Gran*, 2001]. Unfortunately, finding an indication of a flow with a known return time is exceedingly difficult in ungauged bedrock rivers. In order to assign an uncertainty to discharges that formed channel scour lines, we use an empirical relationship for at-a-station channel width derived from gauged rivers to estimate the width of the largest and smallest flood likely to set observed high scour marks. At-a-station channel width ( $w_a$ ) is modeled by the following:

$$w_a = k_a Q^a, \quad (5)$$

where  $k_a$  and  $a$  are empirical constants. The maximum value of  $a$  is 0.26 for alluvial channels [*Knighton*, 1998, and references therein]. Given that bedrock rivers should have smaller widths due to greater bank strength, we consider this exponent to be an upper limit on width estimates that maximizes the sensitivity of width to discharge. At three sites, we calculate the width of the largest event likely to establish high scour indicators using the maximum discharge for 2001–2002. The 2001 and 2002 monsoon seasons are selected because they are the only years for which complete discharge data are available at two of the three sites. The calculation is done for two catchments similar in size to those measured for width scaling, Danaque and Temang (6 and 19 km<sup>2</sup> respectively), and a larger catchment, Khudi (130 km<sup>2</sup>) (Figure 1). Given the rapidly growing vegetation and consistent summer rainfall in Nepal, most of our indicators of high scour are likely to have been established within the last 2–3 years, such that it is reasonable to use this 2-year discharge record. The discharge with a return time of three weeks during the monsoon is used to estimate the width of the smallest event likely to establish a high scour mark. The selection of the 3-week discharge is somewhat arbitrary, but given the observed frequency of high discharges ( $\leq 10$  events/monsoon season: see below), this defines an acceptable lower boundary. We estimate a 10–20% difference in width between the large and small discharge events (Table 1). Because this is the largest source of error, we assign a 20% total uncertainty to channel width measurements.

#### 4.3. Estimating Discharge

[15] Although discharge data are available at 10 gauging stations in the Marsyandi catchment, only two were on small tributaries of the size studied for width variations. Given that variation in bedrock channel width is more likely related to discharge than drainage area, we developed a method for estimating average monsoon discharge at a channel-width measurement site based on point rainfall data. First, the correlation between rainfall and discharge was verified in the Khudi catchment using data from a dense network of 9 weather stations in the 130 km<sup>2</sup> catchment and from a stream gauge at the outlet. Half-hourly rainfall data were initially converted to daily rainfall data which were then areally averaged using a Thiessen weighted average

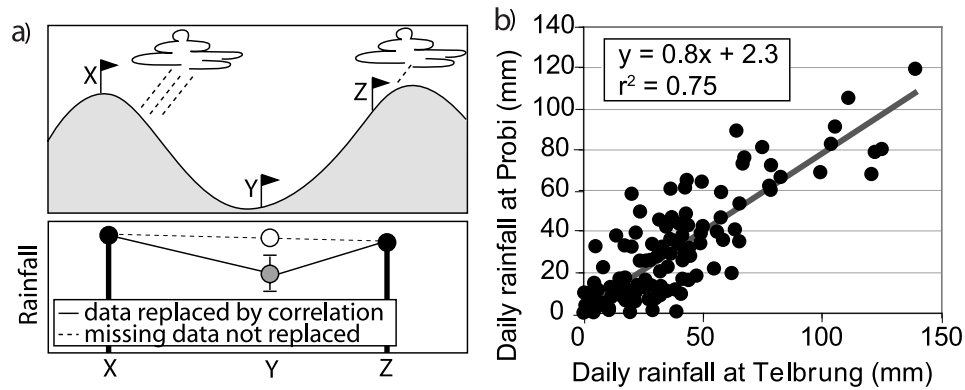


**Figure 3.** (a) X, Y, and Z represent rain gauges in mountainous terrain. Because rainfall varies with elevation, areally averaged rainfall is more accurate if missing point data are estimated. When no data exist for station Y, interpolating between X and Z will overestimate valley precipitation. (b) Representative correlation between a ridgetop station (Telbrug: elevation 3168 m) and a valley bottom station (Probi: elevation 1495 m). Each station is correlated with three others, with the best correlation used to replace missing station data.

[Dunne and Leopold, 1978]. Because many stations had at least a few days with missing rainfall data, each station was correlated to three nearby stations, and the best correlation was used to estimate missing data (Figure 3). When areally averaging rainfall, estimating missing data is preferable to simply omitting a station and interpolating among the remaining stations because of the dependence of rainfall on topography in the study area. Commonly, rainfall on ridges was 10–20% greater than in nearby valleys (Figure 3). Rainfall was also smoothed temporally. Five-day rainfall is strongly correlated to discharge on the sixth day (Figure 4a). Smoothing rainfall over periods longer than 5 days initially yields negligible improvement, and eventually weakens the correlation between rainfall and discharge (Figure 4c). Most rainfall events occur at night, explaining why the optimal window spans at least 2 days [Barros et al., 2000]. The length of the optimal window most probably reflects the fact that runoff processes take place over a handful of days, that prolonged rains exceed the regolith

field capacity [Gabet et al., 2004a], and therefore that consecutive rainy days lead to the highest discharges. The Khudi catchment is much larger (130 km<sup>2</sup>) than the catchments studied for channel-width scaling, and runoff processes are likely to be at least as rapid in the smaller catchments because of shorter runoff pathways.

[16] After establishing the relationship between rainfall and discharge, an isohyetal map was used to assign a mean annual monsoon rainfall to each drainage basin. The mean monsoon rainfall rate (L/T) and drainage area, extracted from the 90-m DEM, (L<sup>2</sup>) are combined and used as a proxy for mean monsoon discharge (L<sup>3</sup>/T) [Dunne and Leopold, 1978]. An analogous technique was used to calculate discharge during individual 5-day storms. We reduced the rainfall-dependent discharge estimate for the entire monsoon by subtracting a volume of water lost owing to evapotranspiration based on elevation-dependent values of evapotranspiration for Nepal [Lambert and Chitrakar, 1989]. Because the large storms we examined deliver at

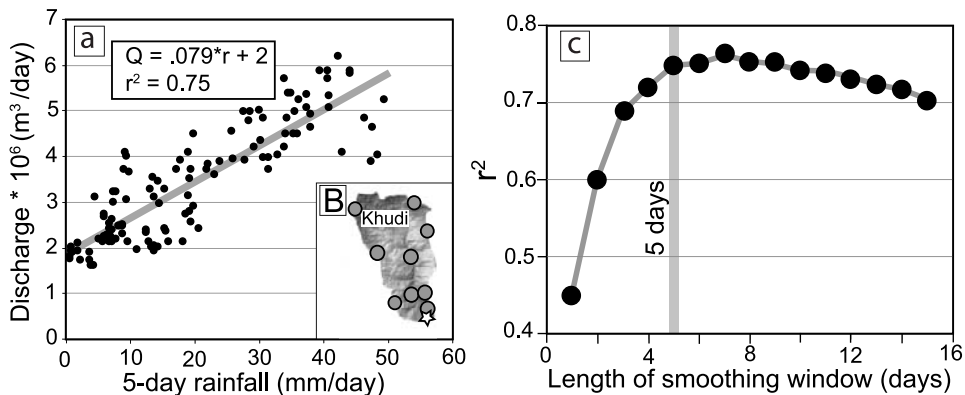


**Figure 4.** (a) Five-day areally averaged precipitation in the Khudi catchment for the period 1999–2003 compared to discharge on the 6th day. (b) Map of Khudi catchment (130 km<sup>2</sup>) showing 9 weather stations (circles) and a stream gauge at the outlet (star). (c) Length of rainfall smoothing window compared to strength of correlation with discharge. Rainfall was smoothed over 1–15 days and compared to discharge on the subsequent day.

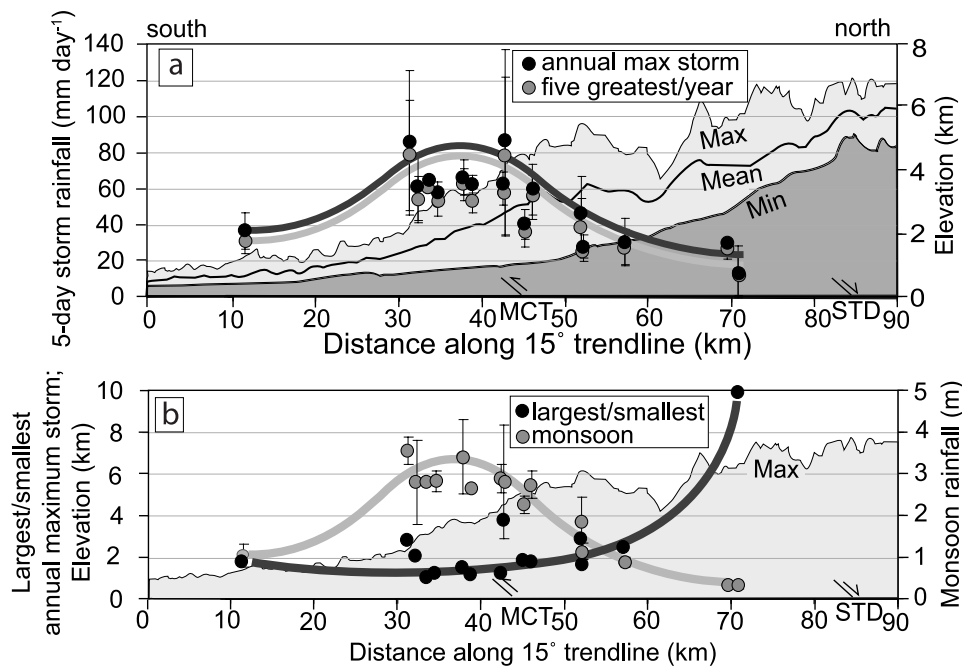


**Figure 5.** (a) Mean of the largest storm in each of 5 years and the mean of the five largest storms in each of 5 years, 1999–2003, plotted above maximum, mean, and minimum topography along a  $15^\circ$  trendline. Error bars represent 1 standard deviation. (b) Largest annual maximum 5-day storm from 1999 to 2003 divided by the smallest annual maximum 5-day storm from the same time period. Also shown is mean annual monsoon rainfall. Hand-drawn thick gray lines highlight the spatial trend in the data.

least a few tens of millimeters of rainfall per day and  $\leq 3.5$  mm/day of rainfall is lost to evapotranspiration, no correction was made for evapotranspiration when estimating daily discharge from 5-day rainfall.

## 5. Results

### 5.1. Monsoon Rainfall: Seasonal Averages and Storms

[17] Fluvial geomorphic work is ultimately driven by precipitation. The arithmetic average of monsoon rainfall varies by over an order of magnitude along the upper Marsyandi River valley for the 5- or 6-year monitoring period (Figure 2c). The standard deviation in monsoonal rainfall at a site is, on average, 20% of the total monsoon rainfall.

[18] Given that channel-forming discharges most likely occur during moderate to large storms [e.g., Leopold and Maddock, 1953; Snyder et al., 2003b], we also investigated the spatial distribution of rainfall during large storms. As a proxy for discharge during these storms, rainfall (1) during the single storm that delivered the largest total rainfall over a 5-day interval in each of 5 years (i.e., 5 storms in all) and (2) during the five storms that delivered the largest to the fifth-largest 5-day total rainfall in each of 5 years (i.e., 25 storms) was averaged over the length of the record (Figure 5a). One striking result, when viewed across the strike of the Himalaya, is that the south-to-north gradient of storm rainfall varies only by a factor of  $\sim 4$ , whereas it varies at the same stations by a factor of  $\geq 11$  for total monsoon rainfall. The standard deviation in annual maximum storm rainfall at a site is, on average, 30%. The data

indicate that large storms penetrate deeper into the mountains than do average storms, thereby reducing discharge differences across the Greater Himalaya in comparison to differences based on the mean monsoonal rainfall.

[19] We also measured interannual storm variability by calculating the ratio of the largest to smallest annual maximum storm at a station over the duration of the rainfall record. The resultant ratios increase sharply at the northern margin of the Marsyandi valley, such that the driest catchments are characterized by the most interannual storm variability (Figure 5b). Additionally, annual maximum series constructed with over 30 years of annual maximum 24-hour storm data from rain gauges at Chame and Khudi (Figure 1b) [Department of Hydrology and Meteorology, 1977, 1982, 1984, 1986, 1988, 1997, 1999, 2001, 2002, 2005a, 2005b] demonstrate that the rate of increase in storm magnitude with respect to return time is more rapid in the north (Figure 6). Thus the 2-year storm is 4–5 times smaller in the drier region compared to the wetter region, whereas the 20-year storm is only 2 times smaller.

[20] The  $>30$ -year record also suggests that rainfall during the period from 1999 to 2003 was representative of rainfall patterns on decadal timescales. For any 5-year window that encompasses a given year and the four preceding years, the ratio of the largest to smallest annual maximum storm between 1971 and 2003 can be compared to the equivalent ratio from our 1999–2004 network data (Figure 7). At Chame (Figure 1b), where mean monsoon rainfall is  $\sim 0.8$  m, ratios of 24-hour storms in a 5-year window vary from 1.6 to 5.3 with a mean of  $3.0 \pm 1.2$ . At Khudi (Figure 1b), where mean monsoon rainfall is much

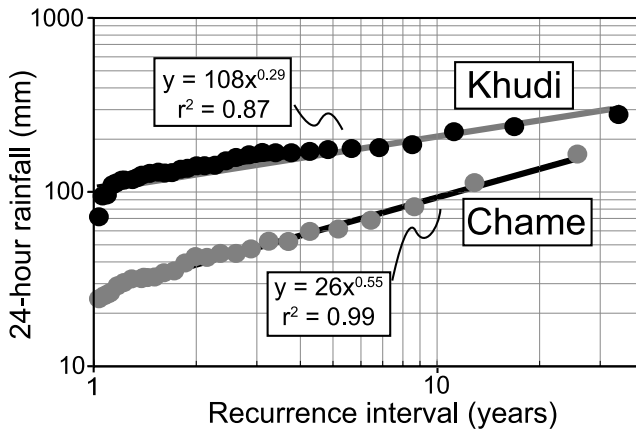


**Figure 6.** Annual maximum series for 24 hour storms at Khudi (1971–2003) and Chame (1978–2003) Data from Nepalese Department of Meteorology and Hydrology. Average annual monsoon rainfall at Khudi is  $\sim 2.8$  m and  $\sim 0.8$  m at Chame. The rate of increase in storm size with respect to return time is higher in relatively dry catchments.

higher ( $\sim 2.8$  m), these ratios only vary from 1.2 to 2.5 with a mean of  $1.9 \pm 0.5$ . Encouragingly, for the period from 1999 to 2003 that coincides with the rainfall data that we exploit in our analysis, year-to-year storm variability hovers near the 30-year mean for both stations (Figure 7), indicating that our data do not include years with anomalously large or small annual maximum storms. Furthermore, the data highlight the far greater interannual variability of the most intense rainfall in relatively dry catchments.

## 5.2. Rock Strength

[21] Channel narrowing may be expected to occur over reaches with stronger rocks because they can support higher wall stresses. Although the Greater Himalayan gneisses in the study area are considered to have relatively uniform strength [Lavé and Avouac, 2001], Schmidt hammer measurements were made in order to assess compressive rock strength across the study area (Figure 2a). Strength measurements (reported in Schmidt hammer units,  $R$ ) at any given site typically vary widely, such that the standard deviation in at-a-site strength is, on average,  $7.5 R$  in the Greater Himalaya. Despite such variability, average rock strength across the Greater Himalaya, where most bedrock channel width measurements were made, is fairly uniform ( $44.2 \pm 4.4 R$ ) (Figure 2b). Rock strength varies more in the Tibetan Sedimentary Series (TSS), ranging from 20 to 50  $R$ . For the sites where we made width measurements in the TSS, more than half yielded Schmidt hammer measurements equivalent to the Greater Himalayan rocks. Six TSS sites have a mean value of 32.1  $R$ ; somewhat lower than in Greater Himalayan rocks. Where studied, the Lesser Himalayan rocks have mean Schmidt hammer measurements of  $44.8 \pm 8.9 R$  which are indistinguishable from the Greater Himalaya. At two Lesser Himalayan channel-width sites, mean rock strength is 30.2  $R$  for foliated schists constituting the banks of the channel, and a measured channel at a nearby site flows over still weaker rock (17.5  $R$ ). The vast majority of channels measured in this study, however, flow

over rocks with uniform strength to within 10%. Where rock strength is more variable, as in the Tethyan and Lesser Himalaya, we expect channel widths to also display greater reach-scale variation.

## 5.3. Channel Width

[22] On the basis of measurements at 71 sites, we find that bedrock channel width scales as a power law function of mean monsoon discharge with a scaling exponent of  $0.38 + 0.092/-0.094$  ( $2\sigma$  error) (Figure 8a). When width is scaled by drainage area, a width scaling exponent of  $0.33 \pm 0.17$  (Figure 8b) is obtained. The  $2\sigma$  errors on this exponent are considerably larger because at any given drainage area, a wide range of mean monsoon discharges occur owing to rainfall differences between catchments (Figure 8d). For the studied channels, the estimated average monsoon discharges span a factor of  $\sim 65$  ( $0.02$  to  $1.3$   $\text{m}^3/\text{s}$ ), whereas drainage areas span a factor of  $\sim 20$  ( $0.6$ – $12.4$   $\text{km}^2$ ). When storm discharge is compared to channel width, a similar width-scaling exponent of  $0.40 + 0.20/-0.17$  is obtained (Figure 8c). The  $2\sigma$  errors for channel width versus storm discharge are greater than for channel width versus mean monsoonal discharge because of the larger errors associated with storm rainfall (Figure 5). Although no statistically significant difference exists among any of the three scaling exponents, the correlation coefficients show notable variation: both storm discharge and mean monsoon discharge are significantly better predictors of width than is drainage area (Figure 8).

## 6. Denudation Rates in the Marsyandi

### 6.1. Impact of Channel Width on Predicted Modern Erosion Rates

[23] In order to estimate how channel characteristics affect erosion across the Marsyandi catchment, we created maps that use specific stream power as a proxy for modern

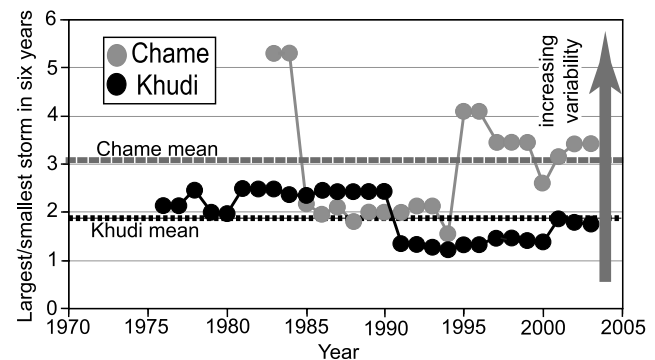


**Figure 7.** Year-to-year variability in annual maximum storms within a moving 5-year window for two locations, Khudi (1971–2003) and Chame (1978–2003). Each point represents the largest annual maximum 24-hour storm to occur in 5 years divided by the smallest annual maximum 24-hour storm to occur in 5 years. The data reported for any given year represent that year and the four previous years. Average annual monsoon rainfall at Khudi is  $\sim 2.8$  m and  $\sim 0.8$  m at Chame. The horizontal lines represent the average of each series.

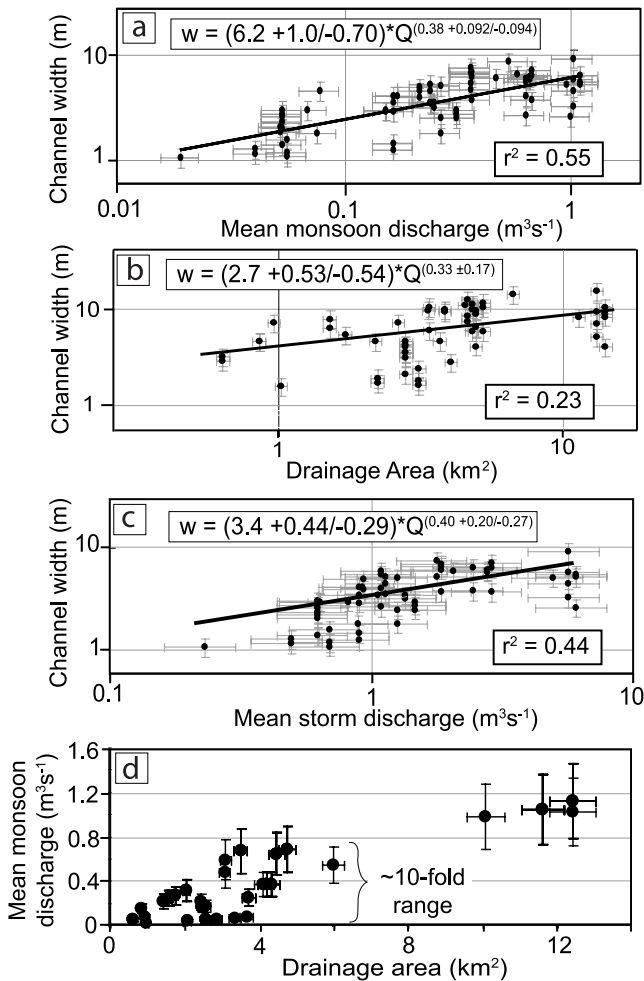


**Figure 8.** (a) Channel width plotted against mean monsoon discharge. X-error bars are the mean standard deviation for total monsoon rainfall at a station (20%). Y-error bars are  $\pm 20\%$ . (b) Channel width plotted against drainage area. X-error bars are 5%. Y-error bars are the same as Figure 8a. (c) Channel width plotted against annual maximum discharge. X-error bars are the mean standard deviation for the annual maximum storm at a station (30%). Y-error bars are the same as Figure 8a. (d) Mean monsoon discharge plotted against drainage area. At any given drainage area, discharge varies widely owing to spatial patterns of precipitation. Because of this, width is more accurately scaled by discharge than drainage area. Note that  $r^2$  values calculated assuming no error in width and discharge/drainage area.

erosion rates. After accounting for bedrock channel width variations, an approximately sixfold south-to-north gradient in specific stream power emerges (Figure 9a), although this same area displays a  $>11$ -fold change in monsoon rainfall and relatively uniform channel gradients in small ( $<20$  km<sup>2</sup>) catchments [Burbank *et al.*, 2003]. Because discharge related to individual multiday storms may be more appropriate for defining specific stream power (Figures 9b and 9c), we also model specific stream power during mean annual maximum discharges.

## 6.2. Probable Channel-Forming Discharge in the Marsyandi Valley

[24] Although we have measured channel widths at recent scour lines, we have no direct proof that the flows that created the scour lines are analogous to those responsible for forming and eroding the channel. Instead, we use erosion rate and discharge data to argue that approximately annual maximum discharges provide reasonable approximations of the channel-forming flows. Erosion rates of 2–4 mm/yr have been measured at millennial scales [Neimi *et al.*, 2005] and at Ma scales [Blythe *et al.*, 2007; Whipp *et al.*, 2007] in the Khudi River watershed (Figure 1b): a wet tributary catchment ( $\sim 3.5$  m rainfall/monsoon) to the Marsyandi. A time series of water and suspended-sediment discharge from this catchment (Figure 10a) displays 1 to 10 flooding events per monsoon season with water discharge  $>6 \times 10^6$  m<sup>3</sup>/day. The floods frequently correspond to high sediment discharges, and roughly 2–8 times/yr, sediment discharge exceeds  $1 \times 10^4$  m<sup>3</sup>/day. Although these thresholds are chosen arbitrarily, the key observation is that each year,  $\sim 1$ –10 events that have a similar magnitude transport most of the sediment through the channel. In the Khudi catchment, the average sediment discharge over the 5 years of observation is equivalent to a catchment-averaged lowering rate of  $\sim 3$  mm/yr [Gabet *et al.*, 2004a; Neimi *et al.*, 2005] when estimates of bed load [Pratt-Sitaula *et al.*, 2007] are added to the observed suspended load. The equivalence between the modern, millennial, and Ma erosion rates suggests that today's high discharges should be proxies for channel-forming events; that is, the channels are adjusted to convey an amount of sediment equal to the long-term sediment load.

[25] Despite fewer high-discharge peaks in drier, more northerly catchments (Figure 10b), the modern sediment discharge is equivalent to an erosion rate of  $\sim 1$  mm/yr (E. J. Gabet *et al.*, Modern erosion rates in the High Himalayas of Nepal, submitted to *Geomorphology*, 2007): a rate approaching the long-term rate inferred from fission track dating [Blythe *et al.*, 2007; Whipp *et al.*, 2007]. Hence we argue that, in both wet and dry catchments, modern channels convey sediment loads analogous to long-term loads and that the observed high-discharge events (1 to 10 per year) are the same ones that shape the channel. There is no need to invoke or expect flows significantly larger than those observed to represent the appropriate channel-forming events.

[26] For rivers that are eroding into bedrock at rapid rates ( $\geq 2$  mm/yr), the overall channel erosion is unlikely to be done by floods larger than those observed nearly every year. Even when Supertyphoon Bilis drenched the rapidly eroding ( $\geq 2$  mm/yr) Taroko Gorge in Taiwan, the average bedrock lowering in the channel was 6–9 mm [Hartshorn *et al.*, 2002]. Bilis was 5 times larger than any other storm in the previous 17 years: an interval over which  $>35$  mm of bedrock would be predicted to have been eroded from the channel. Consequently, Hartshorn *et al.* [2002] inferred that, in Taiwan, several large floods per year are required to sustain or approach the long-term rate of a few mm/yr. We invoke a similar rationale in our Nepalese study: the storms observed over a 5-year period determine the geometry and erosion of the channels that we measured.

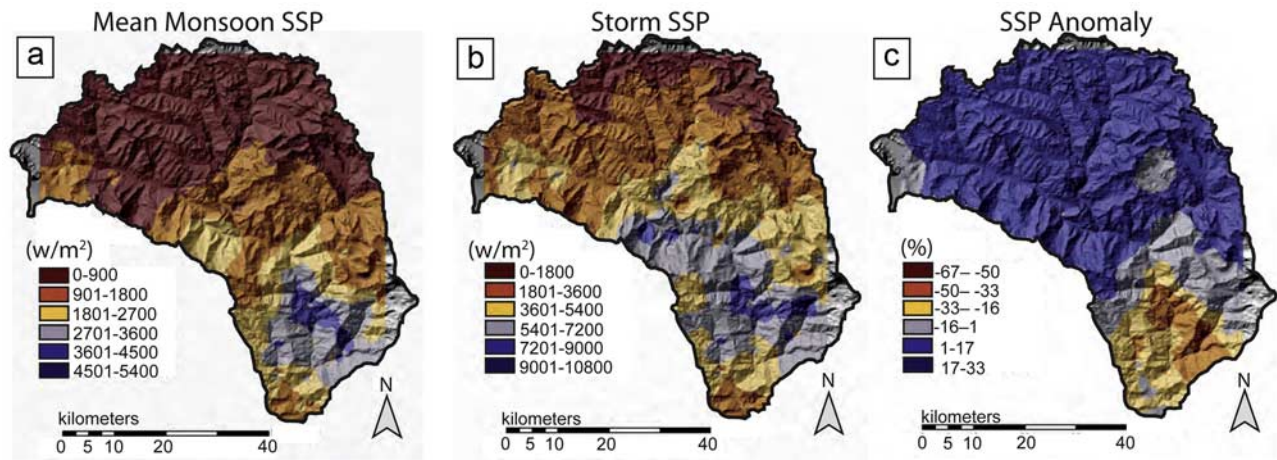


**Figure 9.** (a) Specific stream power (SSP) across the Marsyandi valley for the mean monsoon discharge ( $\text{m}^3/\text{s}$ ). (b) SSP across the Marsyandi valley for the annual maximum discharge ( $\text{m}^3/\text{s}$ ). (c) Difference between SSP during annual maximum discharge and mean monsoon discharge, showing greater relative stream power (positive anomalies) in the north during large storms. Annual maximum stream power is normalized to mean monsoon stream power by reducing each pixel in the annual maximum grid by the ratio of (1) the sum of all pixels in mean monsoon grid to (2) the sum of all pixels in the annual maximum grid, such that both grids have equivalent total stream power. The anomaly map is then created by subtracting mean monsoon stream power from normalized annual maximum stream power. Even after accounting for bedrock channel width adjustments and storm rainfall, significant gradients persist in specific stream power across the Himalaya.

[27] Whereas debris flows are argued to influence, if not control, channel erosion in some steep (0.03–0.10) channels elsewhere [Stock *et al.*, 2005; Stock and Dietrich, 2006], we argue that they have a lesser role in the monsoon-dominated Himalaya. From 1999 to 2004, only 3 debris-charged, high-flow events were observed in the 10 monitored channels in the Marsyandi valley. Although some flows displaced boulders  $>2\text{--}3$  m in diameter, the channel erosion that they caused is unknown. However, as with Supertyphoon Bilis, these infrequent events would have to cause much greater erosion than has been documented for them elsewhere:  $\sim 0.1$  mm/yr [Stock *et al.*, 2005]. Hence we deem it unlikely that relatively rare large debris flows can be primarily responsible for carving steep Himalayan channels.

### 6.3. Erosion Rates Based on Storm Rainfall

[28] We have previously demonstrated that maximum annual storms show an across-strike gradient in rainfall that is less than half as large as that of mean monsoon rainfall (Figure 5), and we interpret that  $\sim 1$ -year floods are likely to drive geomorphic work. Compared to mean monsoon flows, specific stream power during annual maximum storms is more uniformly distributed across the Marsyandi catchment (Figure 9b). To compare the map patterns of stream power quantitatively, we scale the two maps such that sum of all pixels in either map yields the same total stream power. Then an anomaly map is created by subtracting the monsoon stream power from the normalized storm stream power. The entire northern portion of the catchment is characterized by a positive stream-power anomaly (1–17%: Figure 9c), indicating that intense storms penetrate farther into the mountains and reduce the deficit that is predicted on the basis of average monsoon rainfall in the

drier areas. The southern flank of the Greater Himalaya (near Khudi: Figures 1b and 8) is characterized by a strikingly negative stream-power anomaly (–50 to –16%), again emphasizing the more even distribution of specific stream power during annual maximum floods. Nonetheless, a pronounced stream-power gradient persists

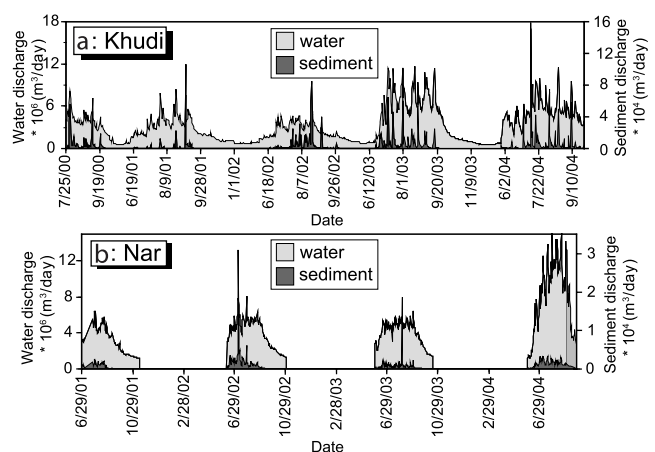


**Figure 10.** (a) Water and suspended sediment discharge for the Khudi catchment ( $130 \text{ km}^2$ ). One to ten floods per monsoon season have water discharge  $>6 \times 10^6 \text{ m}^3/\text{day}$  and two to eight sediment discharge events exceed  $1 \times 10^4 \text{ m}^3/\text{day}$ . (b) Water and suspended sediment discharge for the Nar catchment ( $840 \text{ km}^2$ ). One to eight floods per year have water discharge  $>6 \times 10^6 \text{ m}^3/\text{day}$ , and zero to one sediment discharge events exceed  $1 \times 10^4 \text{ m}^3/\text{day}$ .

across the Himalaya, even after accounting for the distribution of storm rainfall (Figure 9b).

## 7. Effects of Orographic Rainfall on Himalayan Channel Widths and Slopes

### 7.1. Extracting Tectonic Information From Channel Geometry: Previous Work

[29] Because orographic rainfall may cause a rainfall maximum that is significantly offset from a catchment's headwaters [Bookhagen and Burbank, 2006; Roe et al., 2002, 2003] and because an increasing number of studies have inferred spatial patterns of deformation from river topography [Demoulin, 1998; Seeber and Gornitz, 1983], we analyzed how Himalayan-style orographic rainfall gradients are predicted to affect downstream channel geometry on the main stem of the Marsyandi. Recently, two prominent geomorphic indices derived from longitudinal river profiles have emerged, concavity,  $\theta$ , and steepness,  $k_s$ , as useful tools for extracting tectonic information [Snyder et al., 2000; Lavé and Avouac, 2000, 2001; Kirby and Whipple, 2001; Kirby et al., 2003; Wobus et al., 2003, 2005, 2006a; Hodges et al., 2004; Duvall et al., 2004]. Both indices are a function of the rate of change in channel gradient with respect to drainage area (see Snyder et al. [2000] and Wobus et al. [2006a] for a complete discussion). The two indices are derived by plotting channel slope against drainage area on a plot with logarithmic axes. Concavity refers to the slope of a power law regression through the data, and steepness refers to the y-intercept of the regression. Several studies assign a fixed concavity to slope-area data and then relate channel steepness to rock uplift rates, thereby inferring differential rock uplift rates [Kirby et al., 2003; Wobus et al., 2006a].

[30] Previous studies have investigated longitudinal river profiles in the context of rainfall patterns that either increase or decrease toward the headwaters [Roe et al., 2002, 2003]. Along the Greater Himalaya in central Nepal, the highest rainfall typically occurs between 2 and 3 km elevation, where relief and elevation abruptly increase [Bookhagen and Burbank, 2006]. This maximum is typically offset from the highest topography by 10s of kilometers and can be >50 km from the headwaters of trans-Himalayan catchments (Figure 2c). Moreover, the rainfall maximum typically coincides with a transition zone of decreasing normalized steepness in the downstream direction of the trunk rivers [Wobus et al., 2006a]. Wobus et al. [2005, 2006a] argued that most of the observed steepness change results from differential uplift due to slip along an active, surface-breaking thrust south of the Main Central Thrust, and suggested that focused monsoon rainfall may have a second-order influence on channel steepness in this region.

### 7.2. Predicting the Downstream Channel Geometry

[31] In order to separate the rainfall-discharge effects from tectonic forcing, we developed two sets of models of longitudinal river profiles and channel characteristics for catchments, some of which have Himalayan-style rainfall distributions. In the first set, channel geometry was predicted from flow accumulation models for discharge and compared to observed channel geometry along the main stem to test for a relationship between rainfall and channel

geometry. In the second set, a more simplified discharge model was used to explore how rainfall affects channel geometry in an idealized Himalayan catchment.

[32] In the first set of models, discharge along the Marsyandi was modeled using a DEM-derived flow accumulation for the Marsyandi, weighted by the spatially varying, mean monsoon rainfall data from 1998 to 2005, remotely sensed by the Tropical Rainfall Measuring Mission (TRMM) (Figure 11a) [Bookhagen and Burbank, 2006]. This was compared to a second discharge model weighted by the average TRMM monsoon rainfall, distributed uniformly across the entire catchment.

[33] In the second set of models, an average Himalayan catchment shape (based on 10 nearby catchments) was convolved with drainage area and three different rainfall distributions (Figures 12a–12e). One rainfall distribution mimics that in the Himalaya, where the rainfall maximum occurs well downstream of the drainage divide [Roe et al., 2003; Bookhagen and Burbank, 2006], one is more typical of smaller mountain ranges where the rainfall maximum is located near the drainage divide [Roe et al., 2003], and one ignores orographic controls, distributing precipitation uniformly over the catchment, such that discharge is a linear function of upstream catchment area (Figure 12c). All three models deliver the same total volume of rain to the catchment.

[34] For both sets of models, predictions of downstream channel width were made with our observed width-scaling relationship ( $w = 6.2 Q^{0.4}$ ). Channel gradient was predicted using the following restatement of equation (2):

$$S = (U/K)^{1/n} Q^{-m/n}. \quad (6)$$

Rock uplift ( $U$ ), which is approximated from fission track cooling ages [Blythe et al., 2007], is equivalent to erosion ( $E$ ) in equation (2). Therefore implicit in equation (6) is the assumption of a topographic steady state whereby rock uplift and erosion are in balance. In addition to discharge, the values of  $K$ ,  $m$ , and  $n$  are required to predict slope. We follow Roe et al. [2002, 2003] and set  $m = 1/3$ ,  $n = 2/3$ , and  $K = 4 \times 10^{-5}$  [Stock and Montgomery, 1999]. We assume a spatially uniform rock-uplift rate of 3 mm/yr, a reasonable estimate for our field area within the Greater Himalaya [Burbank et al., 2003; Blythe et al., 2007; Whipp et al., 2007]. Absolute values of channel width and slope are sensitive to the selected rock uplift rate; however, qualitative changes in these two model outputs are not (Figure 11d). In order to compare the influence of rock uplift and focused rainfall on channel steepness near the MCT, we implemented a spatial change in tectonic forcing (from 3 mm/yr to 0.5 mm/yr at the downstream end of the high-rainfall zone), thereby mimicking the transition in rock-uplift rates that occurs across the MCT [Blythe et al., 2007; Huntington et al., 2006].

### 7.3. Model Results

[35] The Marsyandi-specific models predict contrasting patterns in downstream discharge as a function of the imposed rainfall distribution. Spatially uniform rainfall produces an early upstream rise in discharge (at  $\sim 30$  km) and then a tapering in the rate of increase in discharge after  $\sim 90$  km. The taper results from the triangular shape of the

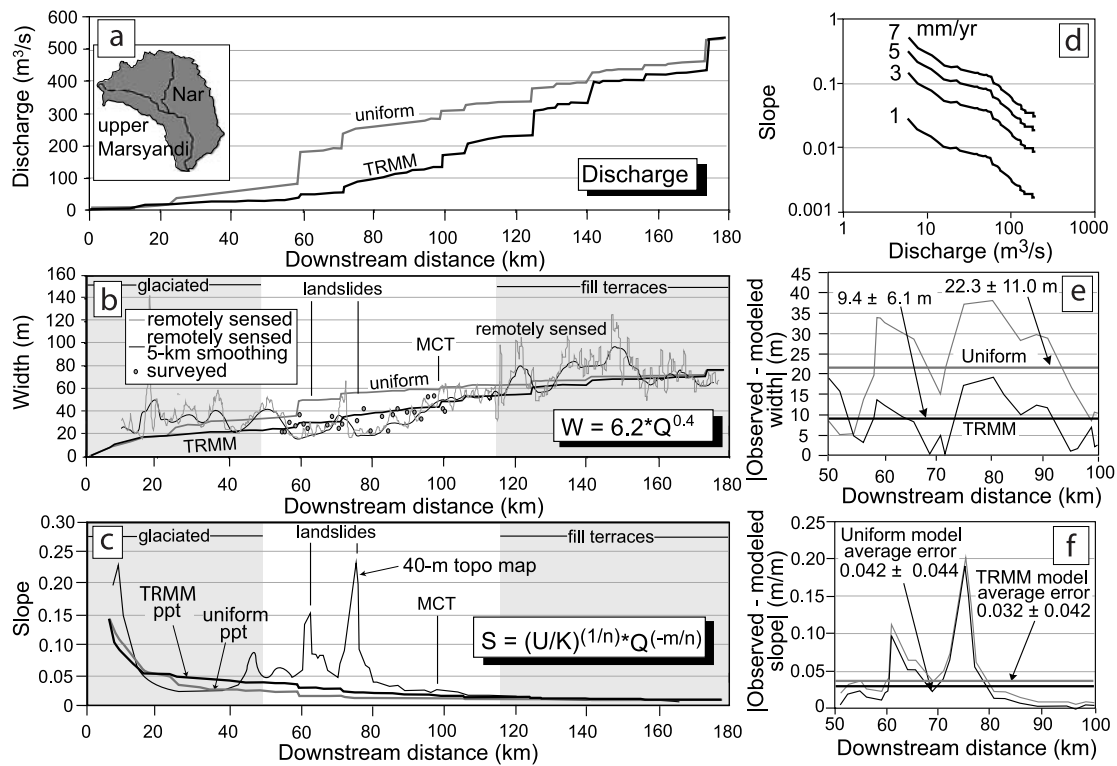


**Figure 11.** (a) Rainfall-weighted flow accumulation models for discharge on the Marsyandi River. The black line is weighted by TRMM data averaged from 1998 to 2005. The gray line is weighted by the average of the TRMM data (0.8 m/monsoon). (b) Channel widths ( $w = 6.2 * Q^{0.4}$ ) compared to observed values [from Lavé and Avouac, 2001]. The thick gray line shows remotely sensed channel widths and the thick black line shows remotely sensed channel widths smoothed over 5 km. Those data are supplemented with measurements made in the field (points). (c) The thick black line shows channel slope predicted by equation (6) using on TRMM rainfall derived discharge. The thick gray line shows channel slope predicted by equation (6) using uniform rainfall derived discharge. Both curves are compared to slope measured from a 40-m topographic map (thin black line). (d) The influence of rock uplift rates on channel gradient. The black lines show channel slope against drainage area predicted for various rock uplift rates. (e) Absolute value of the difference between observed width and modeled width downstream of the previously glaciated portion of the valley and upstream of the MCT. The gray and black lines represent the average mismatch between observed and modeled widths based on uniform rainfall and TRMM rainfall, respectively. (f) Absolute value of the difference between observed channel slope and modeled channel slope downstream of the previously glaciated portion of the valley and upstream of the MCT. The gray and black lines show the average mismatch between observed and modeled channel slope based on uniform rainfall and TRMM rainfall, respectively.

lower half of the Marsyandi catchment (see inset, Figure 11a). For the orographic rainfall model, the rise in discharge begins farther downstream and is more sustained. Increases in discharge at tributary junctions are muted in the upper part of the catchment and amplified in the lower part of the catchment in the orographic rainfall model compared to the uniform rainfall model. Model-predicted width and slope follow these discharge trends. We compared the modeled to the observed channel width and slope to assess whether channel geometry is better predicted after accounting for orographic rainfall (Figures 11b and 11c). Channel width measurements were taken from Lavé and Avouac [2001] and based on a variety of topographic data, including DEMs, SPOT imagery, topographic maps, and air photos. The remotely sensed data were supplemented with field measurements, made with a laser range finder, from kilometer 57 to 102 at  $\sim 1$  km intervals. Downstream slope was

measured from 40-m contour interval topographic maps (Figures 11b and 11c).

[36] In the idealized catchments (Figure 12a), Himalayan-style orographic rainfall distributions are predicted to cause pronounced differences in downstream discharge and channel geometry compared to the other modeled rainfall distributions (Figures 12f and 12g). The Himalayan-style orographic rainfall model induces spatially abrupt changes in discharge, channel width, and gradient as opposed to the other two models (Figures 12f and 12g). Plots of channel gradient against drainage area show that Himalayan-style orographic rainfall produces a sharp increase in concavity in the longitudinal river profile in the zone affected by highest rainfall (Figures 12f and 12g). Importantly, steepness decreases significantly on the downstream side of the zone of high concavity by a factor of  $\sim 2$ . This change is caused solely by orographic rainfall and is independent of any

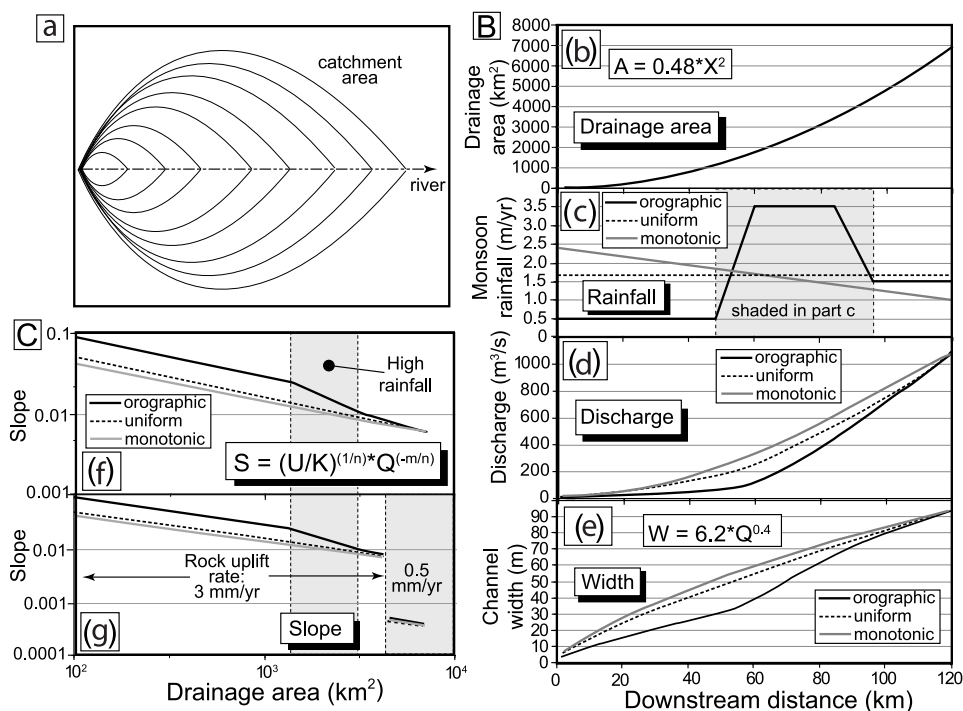


**Figure 12.** Results of numerical modeling of downstream channel geometry. (a) The model catchment is subdivided into 50 self-similar nested catchments, spaced at equal downstream intervals. Catchment shape is based on 10 catchments in or near the Marsyandi valley. (b) Relationship between drainage area and downstream distance based on  $A = 0.48 \cdot X^2$ . (c) Rainfall distributions used to predict downstream discharge. Black curve represents a Himalayan-style orographic rainfall gradient, with the rainfall maximum downstream of the drainage divide. Gray curve represents a rainfall distribution for a smaller mountain range with the rainfall maximum at the drainage divide [e.g., *Roe et al.*, 2002, 2003]. Dashed curve represents a spatially uniform rainfall distribution. (d) Downstream discharge predicted by convolving drainage area and rainfall. (e) Channel width modeled using the relationship in Figure 8 and the discharge models above. (f) Channel gradient versus drainage area. The zone in gray is from 60 to 96 km downstream and corresponds to the zone of high orographic rainfall. A corresponding zone of high concavity is predicted to occur. (g) Channel gradient versus drainage area. The break in the curve corresponds to a decrease in rock uplift rates from 3 mm/yr to 0.5 mm/yr in the downstream direction.

change in tectonic forcing. In contrast, a sixfold change in rock uplift rates at the downstream end of the zone of orographic rainfall induces a more than tenfold change in steepness values (Figures 12f and 12g).

#### 7.4. Channel Geometry as an Indicator of Changing Boundary Conditions

[37] Much of the considerable variation in channel width and gradient can be interpreted in the context of known perturbations to the Marsyandi. In the first 50 km, measured channel gradient is much lower than the models predict (Figure 11b). The modern Marsyandi has alluvial banks in this portion of the catchment, where field evidence suggests that glaciers were present during the last glacial maximum. At  $\sim 63$  and  $\sim 76$  km downstream, pronounced minima in remotely sensed valley width correspond to maxima in channel gradient. Large landslides spilled into the valley and dammed the Marsyandi at both of these locations. The alluviated reaches upstream of both landslide dams are characterized by gentle, wide channels. The river is steep and narrow where it incises the landslide material. Another, smaller landslide is located at  $\sim 87$  km downstream and exerts a similar, but more subtle, influence on channel width

and gradient. Although we model uniform rock uplift throughout the Marsyandi catchment, thermochronologic ages indicate differential uplift due at least in part to Quaternary slip on the Main Central Thrust [*Blythe et al.*, 2007; *Huntington et al.*, 2006] and possibly on nearby faults [*Lavé and Avouac*, 2001; *Wobus et al.*, 2003, 2005; *Hodges et al.*, 2004]. Below the MCT, the Marsyandi valley widens and is alluviated, suggesting a pronounced decrease in rock uplift rates. This transition is clearly visible in the remotely sensed channel-width measurements and occurs at  $\sim 115$  km, downstream of which width rapidly increases from  $<60$  m to  $\sim 80$  m. Lower rates of rock uplift are also expected to cause gentler channels (Figures 12f and 12g), and previous workers have noted a decrease in channel steepness downstream of the MCT [*Hodges et al.*, 2004; *Wobus et al.*, 2005]. Despite the noise in measured width for the Marsyandi, if we only consider the region that lacks persistent alluvial banks, we find that channel width is better predicted when discharge is based on orographic rainfall (Figure 11e). Perturbations to the downstream channel gradient along the Marsyandi render a comparison of the slope models inconclusive (Figure 11f). If the assumptions made about the

**Table 2.** Correlations Between Channel Width and Channel Slope for Selected Discharge Bins<sup>a</sup>

Discharge, m <sup>3</sup> /s	n	Power Law Exponent	r <sup>2</sup>
0.0–0.1	18	0.36	0.34
0.1–0.2	8	0.084	0.064
0.2–0.3	12	−0.016	0.0015
0.3–0.4	11	−0.017	0.079
0.4–0.5	1	n/a	n/a
0.5–0.6	3	0.88	0.94
0.6–0.7	9	−0.16	0.021
0.7–0.8	0	n/a	n/a
0.8–0.9	0	n/a	n/a
0.9–1.0	1	n/a	n/a
1.0–1.1	5	−0.70	0.41
1.1–1.2	3	−0.11	0.27
0.0–1.2	71	−0.20	0.11

<sup>a</sup>Reach average channel width and channel gradient measured at the reach scale were binned by discharge and compared using a power law regression. In general, almost no correlation between the two variables exists. Each discharge bin spans 0.1 m<sup>3</sup>/s of mean annual monsoon discharge. Reach average channel widths and reach-scale channel gradient were also compared across all discharge bins (see final row). The second column, labeled ‘n,’ represents the number of measurement sites within each discharge bin. The third column, labeled ‘power law exponent,’ contains scaling exponents for power law regressions between channel width and channel gradient. The fourth column, labeled ‘r<sup>2</sup>,’ shows the strength of the correlation between channel width and channel slope for a power law regression.

boundary conditions controlling channel geometry (i.e., rock uplift rates, substrate erodibility,  $m$ , and  $n$ ) are accurate, then this analysis demonstrates the importance of orographic rainfall patterns in setting bedrock channel geometry, in particular channel width.

### 7.5. Orographic and Tectonic Influences on Channel Geometry

[38] Himalayan rainfall patterns, typified by a midcatchment zone of intense rainfall, induce a midcatchment zone of high concavity. The high-concavity zone is similar in appearance to tectonic perturbations in the longitudinal river profile but is caused solely by spatial variation in rainfall. In regions where changes in tectonic forcing are subtle and rainfall gradients are pronounced, it may be very difficult to separate the two signals. Pronounced changes in tectonic forcing, however, are predicted to be a more important control on river topography than pronounced rainfall gradients, suggesting that even in regions like the Himalaya, river topography may be used to extract tectonic rates. If the tectonic signal in channel geometry is sufficiently strong, then it may be distinguished from rainfall-related perturbations by comparing channel slope to discharge, not drainage area. Such an analysis, however, requires rainfall data with a high spatial (<10 km) resolution [e.g., *Bookhagen and Burbank*, 2006]. Fortunately, such data are becoming increasingly available through satellite observations.

## 8. Discussion

[39] The proposed coupling between geodynamic and surface processes [*Howard et al.*, 1994; *Small and Anderson*, 1995; *Kooi and Beaumont*, 1996; *Willett*, 1999] has brought the mountain river network to the forefront of geomorphic

research. Because fluvial incision rates are dependent upon channel width, the applicability of power law width-scaling relationships that were developed for alluvial channels is a key unknown for mountain rivers. In light of this, field campaigns have been devoted to calibrating the relationship between downstream channel width in bedrock rivers and discharge or upstream area [*Montgomery and Gran*, 2001; *Snyder et al.*, 2000, 2003a; *Duvall et al.*, 2004; *Wohl and Wilcox*, 2004]. Few of these previous studies explicitly focused on regions where both rock strength and pronounced variations in rainfall were well defined. Moreover, many previous studies of bedrock channel width have focused on downstream width-scaling relationships with width measurements spanning orders of magnitude in drainage area [*Montgomery and Gran*, 2001; *Duvall et al.*, 2004]. In this study, we have quantified bedrock channel width in a large, rapidly denuding orogen across drainage basins with threshold hillslopes and within which both lithology and rates of rock exhumation are relatively uniform, but across which pronounced rainfall gradients are evident. Because tributary catchments do much of the geomorphic work in a given landscape, we focused on width scaling in those smaller catchments. Previous work on catchments of a similar size has demonstrated that across an eightfold gradient in rock-uplift rates, a single relationship that scales channel width to discharge appears applicable [*Snyder et al.*, 2003a]. We have demonstrated that one width-scaling relationship can be used to model many catchments across a region experiencing highly nonuniform rainfall, as long as either discharge or spatial variations in rainfall are known.

[40] Recent numerical modeling studies hold that bedrock channel width is dependent upon both discharge and channel gradient [*Finnegan et al.*, 2005; *Wobus et al.*, 2006b]. We expect that, at a given discharge, if the channel steepens, flow will accelerate and the channel will become narrower, and in an active tectonic environment, we might expect steepening and narrowing as a response to enhanced rock uplift. Recent work in alluvial and bedrock channels crossing growing folds [*Amos and Burbank*, 2007; *Lavé and Avouac*, 2001] suggests that reductions in channel width, without changes in gradient, represent the initial response to increased rates of rock uplift. If rates of uplift continue to increase downstream, then a minimum in channel width is approached, and subsequently the channel gradient may also steepen to augment erosive power. In field settings where slope has been inversely correlated with width for bedrock rivers, channel slope has been measured over spatial scales on the order of ~10 km or more [*Duvall et al.*, 2004; *Finnegan et al.*, 2005]. At similar scales along the main stem of the Marsyandi, channel width and channel gradient do appear to covary in response to major changes in boundary conditions, such as tectonic forcing or the presence of landslide dams (Figures 11b and 11c). However, at the scale of an individual reach in the small catchments that we surveyed, we found no consistent correlation between width and slope (Table 2). Whereas this might reflect the possibility that width adjustments are enough to modulate channel erosion, we suspect the absence of a systematic relationship results from inherent noise in width data at the reach scale (as in work by *Lavé and Avouac* [2001]). At such limited spatial scales, the internal dynamics

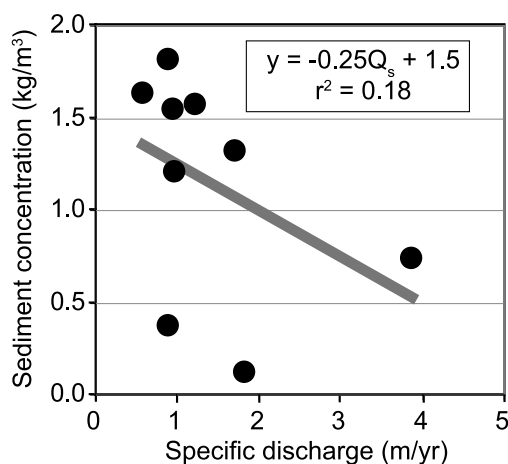


**Figure 13.** Sediment concentration plotted against specific discharge: total monsoon discharge divided by drainage area. Analysis is based on 2–5 years of data from nine different gauging stations. On average, rivers in wet catchments have lower concentrations of suspended sediment.

of bedrock channels (e.g., pools, riffles, and roughness) and the character of the substrate control channel geometries, rather than variations in erosion rates. A significantly larger number of measurements for any given discharge are probably needed to quantify slope-width-discharge correlations at reach scales.

[41] The magnitude of channel-forming discharges in bedrock rivers is not well known and probably differs depending on at least three factors: channel substrate material, sediment supply, and basin hydrology. Given the available hydrologic and geologic data and the apparent need to maintain an erosion rate of 2–5 mm/yr across the Greater Himalaya in central Nepal [Blythe *et al.*, 2007; Burbank *et al.*, 2003; Neimi *et al.*, 2005; Whipp *et al.*, 2007], a strong case can be made that channels tend to actively erode their beds at least every other year. To the extent that discharges driven by individual large storms modulate channel erosion rates, average annual or seasonal rainfall may not be the most appropriate climatic parameter to compare to exhumation rates [e.g., Burbank *et al.*, 2003; Reiners *et al.*, 2003]. Across the region with uniform rates of exhumation in the Marsyandi, spatial gradients in specific stream power, as predicted by storms on the order of the annual maximum storm, are less pronounced than the gradient predicted for specific stream power using seasonal rainfall values (Figure 9b). Nonetheless, a striking north-south, storm-driven specific stream-power gradient exists and is broadly consistent with gradients in modern sediment fluxes, but stands in contrast to the uniform long-term erosion rates across this same area that are inferred from extensive fission track data [Blythe *et al.*, 2007].

[42] The explanation for the absence of a gradient in long-term erosion rates corresponding to the calculated gradient in specific stream power across the Himalaya may reside in several different realms. First, modern or Holocene rainfall patterns may not mimic the average pattern of rainfall over the past 1 Ma. Unless the organization of atmospheric systems (the monsoon) or Himalayan topography and

drainage divides experience a massive change over this interval, however, orographic rainfall will always be greater on the southern flank of the range, far south of the catchment headwaters. Moreover, comparison of modern and past snow lines shows a steeper south-to-north snow line gradient during glacial times [Burbank *et al.*, 2003] and suggests a more pronounced glacial climatic gradient than at present. In comparison to the northern flank of the range, this should consistently enhance fluvial erosion on the southern flank. Second, efficient glacial erosion [Hallet *et al.*, 1996] during times of expanded Pleistocene glaciers might dominate the long-term denudation history in drier, but higher and more heavily glaciated areas, such as the north side of the Himalaya. During interglacial times, such as at present, this effect would be minimized. Third, the role of bed load in modulating channel erosion [e.g., Sklar and Dietrich, 2004] is undefined in these rivers: we have no modern bed load data. Our sediment discharge data, despite their noise and sparse numbers, suggest that suspended-load concentrations are greater in drier areas than in wetter ones (Figure 13). If Himalayan rivers are underloaded with respect to sediment, higher bed loads might drive more efficient channel erosion in drier areas. Fourth, at high rates of erosion (>1 mm/yr), closure temperatures that scale with cooling rates [Reiners, 2005] and larger relative uncertainties on very young fission track ages introduce increasing amounts of ambiguity into erosion-rate calculations [Whipp *et al.*, 2007] and might mask modest spatial variations in rates in the upper Marsyandi catchment. Finally, rainfall may not be the dominant control on patterns of exhumation in the Marsyandi. Spatially uniform vertical transport of rocks above a planar, crustal-scale ramp beneath the Greater Himalaya may be the first-order control on spatial patterns of exhumation [Burbank *et al.*, 2003; Godard *et al.*, 2006].

[43] Extracting tectonic information from river topography can be a powerful neotectonic tool for understanding spatial patterns of deformation and predicting geologic hazards [e.g., Kirby *et al.*, 2003]. The quality of analyses that depend on geomorphic indices of channel concavity and steepness will only be improved by a more complete understanding of the controls on downstream channel gradient. For example, peak monsoon rainfall in the Himalaya, rather than systematically increasing toward a catchment's headwaters, is persistently offset south of the range crest. Such a pattern exerts a first-order control on downstream discharge and channel geometry which differs markedly from catchments for which rainfall gradually increases toward the headwaters. For catchments with strong orographic rainfall gradients, changes in channel slope and steepness can be independent of any changes in rock uplift or erosion and may confound attempts to extract reliable tectonic inferences, especially in regions where tectonic gradients are relatively subtle.

## 9. Conclusions

[44] Whereas spatially uniform rock strength and long-term erosion rates characterize the Greater Himalaya in Marsyandi valley of central Nepal, Himalayan topography creates pronounced rainfall gradients. Such gradients facilitate attempts to quantify the influence of rainfall patterns on

channel width and gradient in the context of an evolving landscape.

[45] 1. An analysis of small Himalayan catchments (<15 km<sup>2</sup>) indicates that the primary control on bedrock channel width is discharge. No single scaling factor that relates catchment area to discharge can be validly applied in regions with pronounced orographic rainfall gradients. Other methods of modeling discharge, such as using stream gauges or combining observed or modeled rainfall and drainage area, are preferable.

[46] 2. The appropriate value of the width-scaling exponent with respect to discharge is ~0.4 in bedrock rivers. This is lower than the commonly accepted exponent in alluvial rivers and suggests that greater bank strength in bedrock rivers causes them to be narrower. This width-scaling exponent can be used to model catchments across a region, regardless of the amount of rainfall they receive, so long as rainfall or discharge is known and other boundary conditions remain constant. The width-scaling exponent is valid across large, rapidly denuding orogenic landscapes. For a given catchment size, bedrock channels are narrower in drier areas, thereby focusing stream power on a smaller area of bedrock. Such width adjustments reduce, but do not eliminate, the mismatch between Quaternary exhumation across the Annapurna Himalaya versus estimated erosion rates that are linearly dependent on modern rainfall gradients.

[47] 3. Average seasonal rainfall does not necessarily mimic the spatial distribution of the storm events that drive erosion. We estimate that events with annual to subannual return periods dominate channel erosion in the Himalaya. In comparison to monsoonal averages, individual large storm events penetrate farther into the Himalaya and can deliver significant moisture to normally dry catchments. Annual maximum storm rainfall varies by a factor of ~4 across the study area, whereas monsoon rainfall varies by a factor of >10. Gradients in monsoon rainfall may significantly overpredict spatial gradients in erosion rates in the Himalaya. Furthermore, greater interannual variability in maximum annual rainfall intensity is observed in dry catchments.

[48] 4. In catchments where the rainfall maximum occurs downstream of the headwaters, longitudinal river profiles can develop zones of high concavity and changing channel steepness in direct response to orographic rainfall gradients. Because such changes can be unrelated to variations in rates of rock uplift or rock strength, they need to be accounted for before making interpretations about spatial patterns of crustal deformation based on topographic indices. In regions where gradients in tectonic rates are sufficiently strong compared to rainfall gradients, river topography may reliably be used to infer differences in rock-uplift rates.

[49] **Acknowledgments.** This research was funded by NSF grant EAR-9909488. We thank Beth Pratt-Sitaula and Jerome Lavé for providing the empirical data used in Figures 12b–12e and Mike Oskin for GIS assistance. We also thank Tank Ojha and the team at Himalayan Experience for assistance in the field. Thoughtful reviews by Cam Wobus, Alex Densmore, and an anonymous reviewer greatly improved this manuscript.

## References

Amos, C. B., and D. W. Burbank (2007), Channel width response to differential uplift, *J. Geophys. Res.*, *112*, F02010, doi:10.1029/2006JF000672.  
 Anders, A. M., G. H. Roe, B. Hallet, D. R. Montgomery, N. Finnegan, and J. Putkonen (2006), Spatial patterns of precipitation and topography in

the Himalaya, in *Tectonics, Climate, and Landscape Evolution, Penrose Conference Series, Spec. Pap. 398*, edited by S. D. Willett et al., pp. 39–53, Geol. Soc. of Am., Boulder, Colo.  
 Barros, A. P., M. Joshi, J. Putkonen, and D. W. Burbank (2000), A study of the 1999 monsoon rainfall in a mountainous region in central Nepal using TRMM products and rain gauge observations, *Geophys. Res. Lett.*, *27*, 3683–3686.  
 Blythe, A. E., D. W. Burbank, A. Carter, K. Schmidt, and J. Putkonen (2007), Plio-Quaternary exhumation history of the central Himalaya: 1. Apatite and zircon fission track and apatite [U-Th]/He analyses, *Tectonics*, *26*, TC3002, doi:10.1029/2006TC001990.  
 Bookhagen, B., and D. W. Burbank (2006), Topography, relief, and TRMM-derived rainfall variations along the Himalaya, *Geophys. Res. Lett.*, *33*, L08405, doi:10.1029/2006GL026037.  
 Brewer, I. D., D. W. Burbank, and K. V. Hodges (2006), Downstream development of a detrital cooling-age signal: Insights from 40Ar/39Ar muscovite thermo-chronology in the Nepalese Himalaya, in *Tectonics, Climate, and Landscape Evolution, Penrose Conference Series, Spec. Pap. 398*, edited by S. D. Willett et al., pp. 321–338, Geol. Soc. of Am., Boulder, Colo.  
 Burbank, D. W. (2002), Rates of erosion and their implications for exhumation, *Mineral. Mag.*, *66*, 25–52.  
 Burbank, D. W., J. Leland, E. Fielding, R. S. Anderson, N. Brozovic, M. R. Reid, and C. Duncan (1996), Bedrock incision, rock uplift and threshold hillslopes in the northwestern Himalayas, *Nature*, *379*, 505–510.  
 Burbank, D. W., A. E. Blythe, J. Putkonen, B. A. Pratt-Sitaula, A. Barros, and T. P. Ojha (2003), Decoupling of erosion and precipitation in the Himalayas, *Nature*, *426*, 652–655.  
 Colchen, M., P. LeFort, and A. Pecher (1986), *Annapurna-Manaslu-Ganesh Himal*, 136 pp., Cent. Natl. de la Rech. Sci., Paris.  
 Dadson, S. J., et al. (2003), Links between erosion, runoff, variability and seismicity in the Taiwan orogen, *Nature*, *426*, 648–651.  
 Demoulin, A. (1998), Testing the tectonic significance of some parameters of longitudinal river profiles: The case of the Ardenne (Belgium, NW Europe), *Geomorphology*, *24*, 189–208.  
 Department of Hydrology and Meteorology (1977), *Climatological Records of Nepal 1971–1975*, vol. I, 366 pp., Kathmandu.  
 Department of Hydrology and Meteorology (1982), *Climatological Records of Nepal 1976–1980*, vol. I, 410 pp., Kathmandu.  
 Department of Hydrology and Meteorology (1984), *Climatological Records of Nepal 1981–1982*, vol. I, 174 pp., Kathmandu.  
 Department of Hydrology and Meteorology (1986), *Climatological Records of Nepal 1983–1984*, vol. I, 187 pp., Kathmandu.  
 Department of Hydrology and Meteorology (1988), *Climatological Records of Nepal 1985–1986*, 232 pp., Kathmandu.  
 Department of Hydrology and Meteorology (1997), *Climatological Records of Nepal 1991–1994*, 378 pp., Kathmandu.  
 Department of Hydrology and Meteorology (1999), *Climatological Records of Nepal 1995–1996*, 323 pp., Kathmandu.  
 Department of Hydrology and Meteorology (2001), *Climatological Records of Nepal 1997–1998*, 193 pp., Kathmandu.  
 Department of Hydrology and Meteorology (2002), *Climatological Records of Nepal 1999–2000*, 194 pp., Kathmandu.  
 Department of Hydrology and Meteorology (2005a), *Precipitation Records of Nepal 1987–1990*, 253 pp., Kathmandu.  
 Department of Hydrology and Meteorology (2005b), *Precipitation Summary of Nepal 2001–2003*, 278 pp., Kathmandu.  
 Dunne, T., and L. B. Leopold (1978), *Water in Environmental Planning*, 818 pp., W.H. Freeman, San Francisco, Calif.  
 Duvall, A., E. Kirby, and D. W. Burbank (2004), Tectonic and lithologic controls on bedrock channel profiles and processes in coastal California, *J. Geophys. Res.*, *109*, F03002, doi:10.1029/2003JF000086.  
 Finnegan, N. J., D. R. Roe, D. R. Montgomery, and B. Hallet (2005), Controls on the channel width of rivers: Implications for modeling fluvial incision of bedrock, *Geology*, *33*(3), 229–232.  
 Gabet, E. J., and T. Dunne (2003), A stochastic sediment delivery model for a steep Mediterranean landscape, *Water Resour. Res.*, *39*(9), 1237, doi:10.1029/2003WR002341.  
 Gabet, E. J., D. W. Burbank, J. K. Putkonen, B. A. Pratt-Sitaula, and T. Ojha (2004a), Rainfall thresholds for landsliding in the Himalayas of Nepal, *Geomorphology*, *63*, 131–143.  
 Gabet, E. J., B. A. Pratt-Sitaula, and D. W. Burbank (2004b), Climatic controls on hillslope angle and relief in the Himalayas, *Geology*, *32*(7), 629–632.  
 Godard, V., J. Lavé, and R. Cattin (2006), Numerical modeling of erosion processes in the Himalayas of Nepal: Effects of spatial variations of rock strength and precipitation, in *Analogous and Numerical Modeling of Crustal-Scale Processes*, edited by S. J. H. Buiter and G. Schreurs, *Geol. Soc. Spec. Publ.*, *253*, 341–358.

- Hallet, B., L. Hunter, and J. Bogen (1996), Rates of erosion and sediment evacuation by glaciers: A review of field data and their implications, *Global Planet. Change*, *12*, 213–235.
- Hancock, G. S., R. S. Anderson, and K. X. Whipple (1998), Beyond power: Bedrock river incision process and form, in *Rivers Over Rock: Fluvial Processes in Bedrock Channels*, *Geophys. Monogr. Ser.*, vol. 107, edited by K. J. Tinkler and E. E. Wohl, pp. 35–60, AGU, Washington, D. C.
- Hartshorn, K., N. Hovius, W. B. Dade, and R. L. Slingerland (2002), Climate-driven bedrock incision in an active mountain belt, *Science*, *297*, 2036–2038.
- Hodges, K. V., R. R. Parrish, and M. P. Searle (1996), Tectonic evolution of the central Annapurna Range, Nepalese Himalayas, *Tectonics*, *15*(6), 1264–1291.
- Hodges, K. V., C. Wobus, K. Ruhl, T. Schildgen, and K. X. Whipple (2004), Quaternary deformation, river steepening, and heavy precipitation at the front of the Higher Himalayan ranges, *Earth Planet. Sci. Lett.*, *220*, 379–389.
- Howard, A. D., W. E. Dietrich, and M. A. Seidl (1994), Modeling fluvial erosion on regional to continental scales, *J. Geophys. Res.*, *99*(B7), 13,971–13,986.
- Huntington, K. W., A. E. Blythe, and K. V. Hodges (2006), Climate change and Late Pliocene acceleration of erosion in the Himalaya, *Earth Planet. Sci. Lett.*, *252*, 107–118.
- Kirby, E., and K. X. Whipple (2001), Quantifying differential rock-uplift rates via stream profile analysis, *Geology*, *29*(5), 415–418.
- Kirby, E., K. W. Whipple, W. Q. Tang, and Z. L. Chen (2003), Distribution of active rock uplift along the eastern margin of the Tibetan Plateau: Inferences from bedrock channel longitudinal profiles, *J. Geophys. Res.*, *108*(B4), 2217, doi:10.1029/2001JB000861.
- Knighton, D. (1998), *Fluvial Forms and Processes: A New Perspective*, 218 pp., Edward Arnold, London.
- Kooi, H., and C. Beaumont (1996), Large-scale geomorphology: Classical concepts reconciled and integrated with contemporary ideas via a surface processes model, *J. Geophys. Res.*, *101*(B2), 3361–3386.
- Lambert, L., and B. D. Chitrakar (1989), Variation of potential evapotranspiration with elevation in Nepal, *Mountain Res. Dev.*, *9*(2), 145–152.
- Lavé, J., and J. P. Avouac (2000), Active folding of fluvial terraces across the Siwaliks Hills, Himalayas of central Nepal, *J. Geophys. Res.*, *105*(B3), 5735–5770.
- Lavé, J., and J. P. Avouac (2001), Fluvial incision and tectonic uplift across the Himalaya of Central Nepal, *J. Geophys. Res.*, *106*(B11), 26,561–26,591.
- Leopold, L. B., and T. Maddock (1953), The hydraulic geometry of stream channels and some physiographic implications, *U.S. Geol. Surv. Prof. Pap.*, *252*, 1–57.
- Molnar, P., and P. England (1990), Late Cenozoic uplift of mountain ranges and global climate change: Chicken or egg?, *Nature*, *346*, 29–34.
- Montgomery, D. R., and J. M. Buffington (1997), Channel-reach morphology in mountain drainage basins, *Geol. Soc. Am. Bull.*, *109*, 596–611.
- Montgomery, D. R., and K. B. Gran (2001), Downstream variations in the width of bedrock channels, *Water Resour. Res.*, *37*(6), 1841–1846.
- Neimi, N. A., M. Oskin, D. W. Burbank, A. M. Heimsath, and E. J. Gabet (2005), Effects of bedrock landslides on cosmogenically determined erosion rates, *Earth Planet. Sci. Lett.*, *237*, 480–498.
- Pratt-Sitaula, B., M. Garde, D. W. Burbank, M. Oskin, A. Heimsath, and E. Gabet (2007), Bedload-to-suspended load ratio and rapid bedrock incision from Himalayan landslide-dam lake record, *Quat. Res.*, *68*, 111–120.
- Raymo, M. E., and W. F. Ruddiman (1992), Tectonic forcing of late Cenozoic climate, *Nature*, *359*, 117–122.
- Reiners, P. W. (2005), Zircon (U-Th)/He thermochronometry, *Rev. Mineral. Geochem.*, *58*, 151–179.
- Reiners, P. W., T. A. Ehlers, S. G. Mitchell, and D. R. Montgomery (2003), Coupled spatial variations in precipitation and long-term erosion rates across the Washington Cascades, *Nature*, *426*, 645–647.
- Roe, G. H., D. R. Montgomery, and B. Hallet (2002), Effects of orographic precipitation variations on the concavity of steady-state river profiles, *Geology*, *30*(2), 143–146.
- Roe, G. H., D. R. Montgomery, and B. Hallet (2003), Orographic precipitation and the relief of mountain ranges, *J. Geophys. Res.*, *108*(B6), 2315, doi:10.1029/2001JB001521.
- Searle, M. P., and L. Godin (2003), The South Tibetan Detachment and the Manaslu Leucogranite: A structural reinterpretation and restoration of the Annapurna-Manaslu Himalaya, Nepal, *J. Geol.*, *111*, 505–523.
- Seeber, L., and V. Gornitz (1983), River profiles along the Himalayan Arc as indicators of active tectonics, *Tectonophysics*, *92*(4), 335–367.
- Sklar, L. S., and W. E. Dietrich (2004), A mechanistic model for river incision into bedrock by saltating bed load, *Water Resour. Res.*, *40*, W06301, doi:10.1029/2003WR002496.
- Small, E. E., and R. S. Anderson (1995), Geomorphically driven late Cenozoic rock uplift in the Sierra Nevada, California, *Science*, *270*, 277–280.
- Snyder, N. P., K. X. Whipple, G. E. Tucker, and D. J. Merritts (2000), Landscape response to tectonic forcing: digital elevation model analysis of stream profiles in the Mendocino triple junction region, northern California, *Geol. Soc. Am. Bull.*, *112*, 1250–1263.
- Snyder, N. P., K. X. Whipple, G. E. Tucker, and D. J. Merritts (2003a), Channel response to tectonic forcing: Field analysis of stream morphology and hydrology in the Mendocino triple junction region, northern California, *Geomorphology*, *53*, 97–127.
- Snyder, N. P., K. X. Whipple, G. E. Tucker, and D. J. Merritts (2003b), Importance of a stochastic distribution of floods and erosion thresholds in the bedrock river incision problem, *J. Geophys. Res.*, *108*(B2), 2117, doi:10.1029/2001JB001655.
- Stock, J. D., and W. E. Dietrich (2006), Erosion of steepland valleys by debris flows, *Geol. Soc. Am. Bull.*, *118*(9/10), 1125–1148, doi:10.1130/B25902.1.
- Stock, J. D., and D. R. Montgomery (1999), Geologic constraints on bedrock river incision using the stream power law, *J. Geophys. Res.*, *104*(B3), 4983–4993.
- Stock, J. D., D. R. Montgomery, B. D. Collins, W. E. Dietrich, and L. Sklar (2005), Field measurements of incision rates following bedrock exposure: Implications for process controls on the long profiles of valleys cut by rivers and debris flows, *Geol. Soc. Am. Bull.*, *117*, 174–194, doi:10.1130/B25560.1.
- Whipp, D. M., Jr., T. A. Ehlers, A. E. Blythe, K. W. Huntington, K. V. Hodges, and D. W. Burbank (2007), Plio-Quaternary exhumation history of the central Himalaya: 2. Thermo-kinematic model of thermochronometer exhumation, *Tectonics*, *26*, TC3003, doi:10.1029/2006TC001991.
- Whipple, K. X. (2004), Bedrock rivers and the geomorphology of active orogens, *Annu. Rev. Earth Planet Sci.*, *32*, 151–185.
- Whipple, K. X., and G. E. Tucker (1999), Dynamics of the stream power river incision model: Implications for height limits of mountain ranges, landscape response timescales and research needs, *J. Geophys. Res.*, *104*, 17,661–17,674.
- Whipple, K. X., G. S. Hancock, and R. S. Anderson (2000), River incision into bedrock: Mechanics and relative efficacy of plucking, abrasion, and cavitation, *Geol. Soc. Am. Bull.*, *112*, 490–503.
- Willett, S. D. (1999), Orogeny and orography: the effects of erosion on the structure of mountain belts, *J. Geophys. Res.*, *104*(B12), 28,957–28,982.
- Wobus, C. W., K. V. Hodges, and K. X. Whipple (2003), Has focused denudation sustained active thrusting at the Himalayan topographic front, *Geology*, *31*(10), 861–864.
- Wobus, C., A. Heimsath, K. X. Whipple, and K. Hodges (2005), Active out-of-sequence thrust faulting in the central Nepalese Himalaya, *Nature*, *434*, 1008–1011.
- Wobus, C. W., K. X. Whipple, E. Kirby, N. Snyder, J. Johnson, K. Spyropolou, B. Crosby, and D. Sheehan (2006a), Tectonics from topography: Procedures, promise, and pitfalls, in *Tectonics, Climate, and Landscape Evolution, Penrose Conference Series, Spec. Pap. 398*, edited by S. D. Willett et al., pp. 55–74, Geol. Soc. of Am., Boulder, Colo.
- Wobus, C. W., G. E. Tucker, and R. S. Anderson (2006b), Self-formed bedrock channels, *Geophys. Res. Lett.*, *33*, L18408, doi:10.1029/2006GL027182.
- Wohl, E. E., and A. Wilcox (2004), Channel geometry of mountain streams in New Zealand, *J. Hydrol.*, *300*, 252–266, doi:10.1016/j.jhydrol.2004.06.006.
- Wohl, E. E., J. N. Kuzma, and N. E. Brown (2004), Reach-scale geometry of a mountain river, *Earth Surf. Processes Landforms*, *29*, 969–981, doi:10.1002/esp.1078.

B. Bookhagen, Department of Geological and Environmental Sciences, Stanford University, Stanford, CA 94305, USA. (bodo@pangea.stanford.edu)

D. Burbank, Department of Earth Science, University of California, Santa Barbara, CA 93106, USA. (burbank@crustal.ucsb.edu)

W. Craddock, Department of Geosciences, Pennsylvania State University, University Park, PA 16802, USA. (bill.craddock@geosc.psu.edu)

E. J. Gabet, Department of Environmental Science, University of California, Riverside, CA 92521, USA. (manny.gabet@ucr.edu)